H3.3-G34R Mutation-Mediated Epigenetic Reprogramming Leads to Enhanced Efficacy of Immune Stimulatory Gene Therapy in Pediatric High-Grade Gliomas

Maria B. Garcia-Fabiani[1,2,3,4*], Santiago Haase[1,2,3*], Kaushik Banerjee[1,2,3*], Brandon McClellan[1,2,3], Ziwen Zhu[1,2,3], Anzar Mujeeb[1,2,3], Yingxiang Li[1,2,3], Jin Yu[3,5], Padma Kadiyala[1,2,3], Ayman Taher[1,2,3], Felipe J. Núñez[1,2,3], Mahmoud S. Alghamri[1,2,3], Andrea Comba[1,2,3], Flor M. Mendez[1,2,3], Alejandro J. Nicola Candia[1,2], Brittany Salazar[1,2,6], Carl Koschmann[7], Fernando M. Nunez[1,2,3], Marta Edwards[1,2,3], Tingting Qin[8], Maureen A. Sartor[8], Pedro R. Lowenstein[1,2,3,9] and Maria G. Castro[1,2,3**].

1 - Department of Neurosurgery, University of Michigan Medical School, Ann Arbor, MI 48109, USA.

2 - Department of Cell and Developmental Biology, University of Michigan Medical School, Ann Arbor, MI 48109, USA.

3 - Rogel Cancer Center, University of Michigan Medical School, Ann Arbor, MI 48109, USA.

4 - Current address: Leloir Institute Foundation, Buenos Aires, Argentina.

5 - Current address: Department of Neurosurgery, Zhongnan Hospital of Wuhan University, Wuhan, 430071, China.

6 - Cancer Biology Graduate Program, University of Michigan Medical School, Ann Arbor, MI, USA.

7 - Department of Pediatrics, Chad Carr Pediatric Brain Tumor Center, University of Michigan Medical School, MI 48109, USA.

8 - Department of Computational Medicine and Bioinformatics, University of Michigan, Ann Arbor, MI 48109, USA.

9 - Department of Bioengineering, University of Michigan, Ann Arbor, MI 48109, USA.

* Equal first authors.

**Corresponding author: mariacas@med.umich.edu

SUMMARY

Pediatric high-grade gliomas (pHGGs) are diffuse and highly aggressive CNS tumors which remain incurable, with a 5-year overall survival of less than 20%. Within glioma, mutations in the genes encoding the histones H3.1 and H3.3 have been discovered to be age-restricted and specific of pHGGs. This work focuses on the study of pHGGs harboring the H3.3-G34R mutation. H3.3-G34R tumors represent the 9-15% of pHGGs, are restricted to the cerebral hemispheres, and are found predominantly in the adolescent population (median 15.0 years). We have utilized a genetically engineered immunocompetent mouse model for this subtype of pHGG generated via the Sleeping Beauty-transposon system. The analysis of H3.3-G34R genetically engineered brain tumors by RNA-Sequencing and ChIP-Sequencing revealed alterations in the molecular landscape associated to H3.3-G34R expression. In particular, the expression of H3.3-G34R modifies the histone marks deposited at the regulatory elements of genes belonging to the JAK/STAT pathway, leading to an increased activation of this pathway. This histone G34R-mediated epigenetic modifications lead to changes in the tumor immune microenvironment of these tumors, towards an immune-permissive phenotype, making these gliomas susceptible to TK/Flt3L immune-stimulatory gene therapy. The application of this therapeutic approach increased median survival of H3.3-G34R tumor bearing animals, while stimulating the development of anti-tumor immune response and immunological memory. Our data suggests that the proposed immune-mediated gene therapy has potential for clinical translation for the treatment of patients harboring H3.3-G34R high grade gliomas.

INTRODUCTION

Central nervous system (CNS) tumors are the leading cause of cancer related deaths in people ranging from 0 to 14 years in the United States (Ostrom et al., 2019). These tumors have an incidence of 5.74 per 100,000 population, and a mortality rate of 4.42 per 100,000 population for malignant tumors (Ostrom et al., 2019). Pediatric high grade gliomas (pHGGs), which include anaplastic astrocytoma (CNS WHO grade III), glioblastoma multiforme (GBM; CNS WHO grade IV), and diffuse midline gliomas (CNS WHO grade IV), are diffuse, infiltrating, and highly aggressive tumors (Jones et al., 2017; Lin et al., 2019; Miklja et al., 2019). Currently, they remain incurable, with a 5-year overall survival of less than 20% (Miklja et al., 2019; Siegel et al., 2016). Despite these adverse statistics, the last decade has been crucial in the understanding of the molecular features of pHGGs (Mackay et al., 2017; Schwartzentruber et al., 2012; Sturm et al., 2012a). One of the breakthroughs in pediatric glioma biology was the discovery of mutations in the histone gene H3. These mutations are involved in glioma development, and their presence correlates with distinct genomic alterations, epigenetic landscapes, CNS locations and clinical features (Bjerke et al., 2013; Mackay et al., 2017; Puntonet et al., 2018; Schwartzentruber et al., 2012; Sturm et al., 2012a; Yoshimoto et al., 2017).

In this study, we focused on the subtype of pHGG harboring a mutation in the histone H3.3 gene *H3F3A*, that changes the glycine at the position 34 to an arginine (H3.3-G34R) or, less commonly, to a valine (Mackay et al., 2017; Schwartzentruber et al., 2012). This mutation is present in 9-15% of pHGGs, is restricted to the cerebral hemispheres, and is found predominantly in the adolescent population (median 15.0 years) (Mackay et al., 2017; Pathak et al., 2015; Schwartzentruber et al., 2012; Sturm et al., 2012a; Wu et al., 2012). G34-mutant pHGGs are characterized by the presence of loss of function mutations in *ATRX/DAXX* and *TP53* genes, and a DNA hypomethylated phenotype (Mackay et al., 2017; Schwartzentruber et al., 2012; Sturm et al., 2012a). The prognosis of these tumors is dismal, with patients displaying a median survival of 18.0 months, and a 2-year overall survival of 27.3% (Mackay et al., 2017).

The understanding of the mechanisms that underlie H3.3-G34R/V subgroup's disease progression in pediatric high-grade gliomas (pHGGs) are not well understood (Korshunov et al., 2016; Sturm et al., 2012b), (Mackay et al., 2018). Presently, the standard of care (SOC) for non-midline pHGGs, irrespective of their H3 status, includes maximum surgical removal followed by targeted radiation. The benefit of chemotherapy in addition to radiation for G34-mutant pHGGs

is still under debate, largely because earlier cooperative group studies did not consistently test and stratify for G34 mutations (Haase et al., 2022).

The implementation of effective immunotherapies for pHGG remains underdeveloped. Recent studies in pediatric high-grade gliomas (HGG) have shown a complex and dynamic interaction between the tumor cells and the immune system (Gonzalez Castro et al., 2023). pHGGs are heterogeneous tumors with a significant portion of the tumor mass consisting of non-malignant cells, such as macrophages, microglia, and dendritic cells, as well as myeloid-derived suppressor cells (MDSCs), which are found extensively in the pHGG TME and have been identified as major contributors to immunosuppression within the tumor microenvironment (Kamran et al., 2018, Alghamri, 2021 #190). Thus, the development of immunotherapies has been limited by several factors, notably the anti-inflammatory tumor microenvironment frequently found in these tumors, which is influenced by many factors, including the specific tumor subtype, the genetic aberrations found within the tumor, and the host immune system.

In recent single-cell transcriptomic studies, G34-mutant pHGGs have been shown to feature a relatively small population of immune cells, unlike adult gliomas that are characterized by a large count of immune cells exhibiting an immunosuppressive phenotype (Chen et al., 2020). However, whether there is a connection between this characteristic and the immune response in this type of pHGG is still unclear. A recent study has documented the impact of germinal G34 mutations on mouse phenotypes (Khazaei et al., 2023). The authors found that the G34-mutant histone leads to a reduction in H3K36me2, which subsequently results in the hindered recruitment of DNMT3A, a DNA methyltransferase, *in cis*. This, in turn, causes hypomethylation in the DNA, particularly impacting the regulatory regions of immune-related genes. This hypomethylation triggers an increase in the expression of these genes, leading to the activation of proinflammatory signals in the brains of G34-mutant mice (Khazaei et al., 2023). These findings correlated with the accumulation of microglia/astrocytes and neuronal depletion in G34-mutant mice.

Understanding the molecular characteristics of the pHGG tumor cells and their interactions with the TME is critical to evaluate the implementation of immunotherapies for G34-mutant pHGG. In this study, we aimed to understand the biological and molecular features of pHGGs harboring H3.3-G34R mutations, as well as its immunological landscape. So far, the tumor immune microenvironment (TME) of pediatric brain tumors has been understudied, holding back the successful development of targeted immunotherapies (Griesinger et al., 2013; Plant et al., 2018; Wang et al., 2019). We generated genetically engineered mouse models (GEMM) of pHGGs

117 harboring the H3.3-G34R mutation, in combination with *ATRX* and *TP53* downregulation, which
118 recapitulates salient features of the human disease (Calinescu et al., 2015),(Haase et al., 2022).
119 A previous study from our lab using this model allowed us to identify that H3.3-G34-mutations
120 drive DNA repair impairment and genetic instability in pHGG, leading to the activation of the
121 cGAS-STING pathway and enhanced anti-tumoral immunological responses (Haase et al.,
122 2022). Thus, in this study, we aimed at characterizing the consequences of the G34-mutations
123 in shaping the immune TME.

124 Using ChIP-Seq and RNA-Seq, we uncovered the molecular landscape of H3.3-G34R pHGG
125 cells, unveiling the consequences of the H3.3-G34R mutation at the epigenetic and
126 transcriptional levels. Our results revealed that the presence of H3.3-G34R correlates with the
127 epigenetic and transcriptional upregulation of pathways related to immune-activation. We show
128 that this correlates with the postraslational activation of the JAK-STAT signaling pathway in
129 G34-mutant cells. Then we studied the immune cell composition of the H3.3-G34R pHGG TME
130 and discovered that H3.3-G34R pHGG have a less immunosuppressive TME with respect to the
131 control group, harboring the wild-type H3.3. Leveraging these differences, we tested the efficacy
132 of Ad-TK/Ad-Flt3L immune stimulatory gene therapy (Alghamri et al., 2021; Ali et al., 2005;
133 Candolfi et al., 2014; Curtin et al., 2009; Kamran et al., 2017; Mendez et al., 2020). We
134 observed an effective anti-tumor CD8 T cell immune response, an increase in the median
135 survival of H3.3-G34R-pHGG bearing animals, and the onset of anti-tumor immunological
136 memory. Collectively, our results uncovered molecular features of H3.3-G34R pHGGs and
137 suggest that immune-stimulatory therapeutic approaches, such as the TK/Flt3L gene therapy,
138 could be considered as an attractive adjuvant treatment for H3.3-G34R pHGGs.

139

140 **RESULTS**

141 **Development of a genetically engineered mouse model for H3.3-G34R pHGGs.**

142 Using the Sleeping Beauty (SB) transposon system, we generated an immunocompetent mouse
143 model for pHGGs harboring H3.3-G34R mutation (H3.3-G34R group) or H3.3-Wt (control group)
144 (Haase et al., 2022). This system allows the *de novo* induction of brain tumors using non-viral,
145 transposon-mediated integration of plasmid DNA into cells of the sub-ventricular zone of
146 neonatal mice by the SB-transposase (Calinescu et al., 2015; Garcia-Fabiani et al., 2020b;
147 Haase et al., 2022; Koschmann et al., 2016a; Núñez et al., 2019; Wiesner et al., 2009) (Figures
148 1, A and S1, A-C). The H3.3-G34R pHGG were modelled by the insertion of plasmid DNAs
149 encoding: i) *NRASG12V* (NRAS activating mutation) (the receptor tyrosine kinase (RTK)–RAS–
150 phosphatidylinositol 3-kinase (PI3K) pathway is activated in a large number of pHGGs
151 (Guerreiro Stucklin et al., 2019; Koschmann et al., 2016b; Mackay et al., 2017; Ney et al., 2020;
152 Paugh et al., 2010; Schwartzentruber et al., 2012)); short hairpin (sh) RNAs against ii) *Atrx* and
153 iii) *Tp53* genes; and iv) the mutated histone H3.3-G34R (H3.3-G34R group) into the mouse
154 brain cells' genome (Figure S1, A) (Haase et al., 2022). As controls, we generated brain tumors
155 encoding *NRASG12V*, shRNA-*Atrx* and shRNA-*Tp53* (H3.3-Wt group) (Figure S1, A-B) as
156 previously described (Haase et al., 2022; Koschmann et al., 2016a).

157 Mice injected with SB plasmids as described above developed tumors, and the G34-mutant
158 GEMM displayed a median survival (MS) of 161 days (Figure 1, A). We were able to verify the
159 development of tumor as the expression of each genetic lesion is coupled to the expression of
160 fluorescent proteins (Figure S1, B).

161 H3.3-G34R expression in the genetically engineered pHGG model was confirmed by
162 immunohistochemistry (IHC) (Figure S2, A-B). These tumors were diffusely infiltrative and
163 hypercellular (Figure S2, D-E). Also, they showed other salient characteristics of pHGG such as
164 pseudopalisades with necrotic areas, microvascular proliferation, hemorrhagic areas,
165 multinucleated giant cells and nuclear atypia (Gianno et al., 2018; Korshunov et al., 2016)
166 (Figure S2, D-E). We confirmed by western blotting that primary cells generated from tumors
167 expressed H3.3-G34R (Figure S2, C). Additionally, we observed that the oligodendrocyte
168 marker OLIG2, a hallmark of these tumors, was downmodulated in the H3.3-G34R pHGG cells
169 (Figure S2, C) (Gianno et al., 2018; Mackay et al., 2017; Sturm et al., 2012a).

170 **The expression of the H3.3-G34R mutation leads to reprogramming of the molecular**
171 **landscape of pHGG cells, upregulating the expression of immune-related genes.**

172 To better understand the effects of H3.3-G34R expression on the transcriptional landscape of
173 glioma cells, we performed RNA-Seq on H3.3-G34R and H3.3-Wt cells extracted from the TME
174 of SB-derived pHGG. Tumor cells were separated from the immune cells (CD45+) and the
175 RNA-Seq analysis was conducted on tumor-enriched cell fractions (Garcia-Fabiani et al.,
176 2020a). Among the 22,828 genes that were measured, 353 were found to be differentially
177 expressed between H3.3-G34R vs H3.3-Wt tumor cells (Fold Change: 0.585, adjusted p value
178 <0.05) (Supplementary Table 1) (Figure 1, C). Amongst the upregulated Gene Ontologies
179 (GOs) in the H3.3-G34R group, we observed terms related to immune-mediated processes,
180 such as "Innate immune response" and "Regulation of adaptive immune response" (Figure 1, B
181 and E). Particularly, we found GOs related to interferon I (IFN-I) (IFNα and IFNβ) and interferon
182 II (IFN-II) (IFNγ) signaling, and several genes involved in these pathways were upregulated in
183 H3.3-G34R tumor cells versus H3.3-Wt tumor cells (Figures 1, B, E and S3, B). The
184 upregulation of type I IFN pathways aligns with previous work from our lab showing that DNA
185 damage deficiencies and genetic instability in G34-mutant pHGG lead to activation of the cGAS-
186 STING pathway in G34-mutant pHGG (Haase et al., 2022) (Figure 1, E). Among the
187 downregulated GOs in the H3.3-G34R group, we found several GOs related to CNS
188 development (Figure S3, A).

189 To validate the conservation of these findings in patients, we retrieved transcriptomic expression
190 data from G34R-mutant versus histone-Wt hemispherical pHGG from the patients' database
191 pedcbioportal and evaluated the expression of JAK/STAT signaling pathway genes. We found
192 that the gene ontology "Positive regulation of peptidyl-serine phosphorylation of STAT protein" is
193 upregulated (Q value = 0.00206) in G34R-mutant patients (Figure S3, C).

194 The H3.3-G34 mutations occur close to a lysine located at the position 36 (H3K36) of the H3.3
195 histone tail. H3K36 can be trimethylated (H3K36me3) and this is regarded as a transcriptional
196 activation mark (Hyun et al., 2017; Schwartzentruber et al., 2012). It has been demonstrated
197 that, even though the H3.3-G34 mutations do not alter the global amounts of H3K36me3, they
198 reduce the H3K36me2 and H3K36me3 deposition in *cis*, and affects the deposition of this
199 epigenetic mark throughout the genome, shaping the transcriptional signature of the cell (Bjerke
200 et al., 2013; Lewis et al., 2013; Mackay et al., 2017). Thus, to test the epigenetic consequences
201 of the H3.3-G34R mutation in relation to histone mark deposition, we analyzed the differential
202 binding of several histone marks throughout the H3.3-G34R and H3.3-Wt pHGG cells'
203 chromatin (Figure 2, A). Using ChIP-Seq, we assessed the binding of H3K4me1, H3K4me3,
204 H3K27ac, H3K36me3 (transcriptional activation marks), and H3K27me3 (transcriptional

205 repressive mark) (Bannister and Kouzarides, 2011), across the genome of H3.3-Wt and H3.3-
206 G34R pHGG cells (Figure 2, A-H). After the reads' alignment and the fulfillment of quality
207 controls, peak calling was performed to identify gene regions differentially enriched in specific
208 histone marks, between H3.3-G34R and H3.3-Wt pHGG cells. Although no differences in global
209 histone mark levels were found between H3.3-G34R and H3.3-Wt pHGG cells by Western blot
210 (Figure S4, D), GSEA of differentially enriched genes in these marks allowed the identification of
211 GO related to pathways or biological processes being epigenetically affected by H3.3-G34R
212 expression (Figures 2, B-C and S4, A-C). When exploring GOs related to the immune system
213 activation/regulation, we observed differentially enriched immune-related GOs associated to
214 H3K27me3 and H3K36me3 deposition (Figure 2, B-C). The H3K27me3 mark, which is
215 associated to transcriptional repression, was enriched in GOs related to the regulation of signal
216 transducer and activator of transcription (STAT) cascade and the activation of T cell-mediated,
217 NK cell-mediated, B cell-mediated and humoral responses in H3.3-Wt cells. On the other hand,
218 in H3.3-G34R pHGG cells, the H3K27me3 mark was enriched in GOs related to leucocyte
219 apoptotic processes (Figure 2, B). Moreover, the H3K36me3 mark, which is associated to
220 transcriptional activation, was enriched in GOs related to the negative regulation of T cell
221 proliferation and activation, and the development of the immune system in H3.3-Wt pHGG cells;
222 whereas this mark was found to be enriched in GOs related to leucocyte chemotaxis, myeloid
223 cytokine production and STAT pathway activation in H3.3-G34R pHGG cells (Figure 2, C).
224 H3K27ac, H3K4me3 and H3K4me1 (Figure S4, A-C) were differentially bound to genes
225 encountered in immune-related GOs. These results indicate that H3.3-G34R affects the
226 deposition of different histone marks across the genome, specifically altering the epigenetic
227 regulation of genes related to an active immune response.

228 Since we found striking differences in histone mark deposition due to the expression of H3.3-
229 G34R (Figure S4, E), we performed an analysis to define chromatin states (CS) at different
230 gene regulatory regions (Figure S4, F-G). CS were determined by the combination and the
231 relative abundance of different histone marks at a particular locus. For example, the CS "active
232 enhancer" was defined by presence of H3K27Ac+H3K4me1 histone marks, or "bivalent/poised
233 transcription start site" by presence of H3K27me3+H3K4me3+H3K27Ac+H3K4me1 histone
234 marks (Bogu et al., 2016; Fiziev et al., 2017) (Figure S4, G). Given that several genes related to
235 IFN-I and IFN-II related pathways were upregulated in H3.3-G34R with respect to H3.3-Wt
236 pHGG cells in the RNA-Seq analysis (Figure 1, B, D-E), we analyzed the epigenetic regulation
237 and the CS changes of genes related to IFNγ signaling and STAT1 pathway activation. IFNγ is
238 a cytokine secreted by activated CD4 and CD8 T cells, as well as by antigen presenting cells,

239 and its pleiotropic function resides on its ability to modulate the expression of numerous genes
240 (Gocher et al., 2022; Kane and Yang, 2010; Schroder et al., 2004). IFNγ canonical signaling
241 pathway involves IFNγ binding to IFNGR1 and IFNGR2, the activation of JAK1 and JAK2, and
242 the phosphorylation of STAT1 (pSTAT1) (Schroder et al., 2004; Castro et al., 2018; Gocher et
243 al., 2022; Schroder et al., 2004). The homodimerization of pSTAT1 forms a complex, which
244 translocates to the nucleus and binds to gamma-activated sites (GAS), increasing the
245 transcription of target genes (Figures 3, A and S5, A) (Schroder et al., 2004).

246 One of these genes is the transcription factor interferon-regulatory factor 1 (*IRF1*), which binds
247 to interferon-stimulated response elements (ISRE) and enhances the transcription of several
248 secondary response genes, such as Class II transactivator (*CIITA*) and Suppressor of cytokine
249 signaling (*SOCS*) which negatively regulates the IFN-γ pathway by inhibiting JAKs and STAT1
250 phosphorylation (Figures 3A and S5, A) (Schroder et al., 2004). CIITA is the mediator of IFNγ-
251 inducible transcription of Major Histocompatibility Complex (MHC) class I and II genes
252 (Muhlethaler-Mottet et al., 1998; Schroder et al., 2004). We found differences in the binding of
253 single histone marks on genes related to STAT-pathway GOs (Figures 2, B-C and S5, B-E), and
254 specifically in the CS of key genes involved in STAT1 signaling (Figures 2, B-E, I and S5, F).
255 The analysis of CS changes between H3.3-G34R and H3.3-Wt pHGG cells revealed
256 transcriptionally-permissive CS for genes related to STAT1 pathway and IFNγ signaling in H3.3-
257 G34R cells, which correlated with the transcriptional data obtained from the RNA-Seq analysis
258 (Figure 3, C) *i.e.*, genes that were shown to be downregulated in H3.3-Wt vs H3.3-G34R pHGG
259 cells by RNA-Seq, were associated to regions with CS related to transcriptional repression in
260 H3.3-Wt cells. For example, we found that *Stat1* (Figure 3, D-E), *Ciita* (Figure 4, A), and MHC-I
261 (Figure 4, C) genes, which were shown to be downregulated in the H3.3-Wt pHGG cells by
262 RNA-Seq (Figure 1, D), were enriched in CS related to gene silencing or repression at specific
263 regions in H3.3-Wt vs H3.3-G34R cells.

264 Overall, the presence of H3.3-G34R has profound effects on the epigenetic landscape of pHGG
265 cells, which is reflected in the distinctive transcriptional profile observed in these tumors by
266 RNA-Seq. Specifically, we observed that H3.3-G34R expression impacts pathways related to
267 immune system processes and IFNy signaling.

268 **STAT1 is postranslationally activated in G34-mutant pHGG**

269 As the RNA-seq performed on tumor cells isolated from the TME showed upregulation of STAT
270 genes and gamma-interferon activated pathways, we hypothesized that interferon-gamma and

271 other cytokines in the G34-mutant pHGG TME stimulate the JAK/STAT pathway. Thus, we
272 evaluated STAT1- phosphorylation (Tyr-705), STAT5a phosphorylation (phospho-Ser780) and
273 JAK2 levels in H3.3-G34-mutant pHGG and H3.3-Wt mouse pHGG cells by western blot. Our
274 results show that the normalized levels of phospho-STAT1-Tyr-705 are increased in G34-
275 mutant pHGG cells compared to their H3.3-Wt in basal conditions and at all the times ($p < 0.01$)
276 after IFNγ stimulation evaluated (Figure 3, F-G). Similarly, STAT5a phosphorylation (phospho-
277 Ser780) normalized and JAK2 levels are levels are increased in G34-mutant tumors compared
278 to their H3.3-Wt counterparts in basal conditions and upon IFNy stimulation (Figure 3, H-J).

279 **The JAK/STAT pathway activity is increased in G34-mutant pHGG after IFNγ stimulation**

280 To characterize in detail the JAK/STAT pathway activity in H3.3-G34-mutant and H3.3-Wt
281 pHGG cells, we analyzed the levels of proteins and their postraslational modifications using an
282 antibody array with 42 antibodies related to the JAK/STAT pathway. We characterized the levels
283 of postranslational modifications and basal proteins in pHGG cells in basal conditions and after
284 stimulation with IFNγ. Under basal conditions, the levels of phosphorylation in proteins
285 associated with postranslational activation of the JAK/STAT pathway are similar in G34-mutant
286 and H3.3-Wt pHGG cells (Figures 3, K and S6, A) but after stimulation with IFNγ, these levels
287 are increased in G34-mutant compared with H3.3-Wt cells (Figures 3, K and S6, B) (with
288 STAT5A (Phospho-Ser780), JAK2 (Phospho-Tyr1007), STAT3(Ab-705), STAT3(Phospho-
289 Ser727), STAT4 (Phospho-Tyr693), MEK1 (Ab-217), Raf1 (Ab-338), MEK1 (Phospho-Ser217)
290 differentially upregulated (Q value <0.05) in IFNγ-treated H3.3-G34R vs H3.3-Wt pHGG cells)
291 (See Supplementary Table #). This indicates that G34-mutant pHGG cells are more sensitive to
292 IFNγ stimulation, which leads to postranslational activation of the JAK/STAT pathway.

293 **H3.3-G34R pHGG cells are sensitive to IFNy stimulation and IFNy-mediated apoptosis**

294 IFNγ, and IFNs in general, are known to have anti-tumor effects (Jorgovanovic et al., 2020). The
295 anti-tumor effects of IFNγ can be either indirect or direct. Indirectly, this cytokine is a powerful
296 mediator of innate and adaptive immune response; whereas directly, it can inhibit tumor cell
297 proliferation and induce tumor cell apoptosis (Gocher et al., 2022; Chawla-Sarkar et al., 2003;
298 Kane and Yang, 2010; Schroder et al., 2004). Thus, we aimed to test if H3.3-G34R pHGG cells
299 were also more sensitive to IFNγ-induced apoptosis. We incubated H3.3-G34R or H3.3-Wt
300 pHGG cells with 200 UI of mIFNγ for 48 hours and then, the proportion of live, late apoptotic,
301 early apoptotic, and necrotic cells was assessed by AnnexinV/DAPI staining (Figure 3, L-M).
302 After IFNγ treatment, we observed a significant reduction in the proportion of live cells in the

303 H3.3-G34R group (p<0.0001) (Figure 3, L-M) . Also, a significant increase (p < 0.0001) in the
304 proportion of early apoptotic cells was observed in the H3.3-G34R group (Figure 3, L-M) . No
305 significant differences were found in the proportion of late apoptotic or necrotic cells in either
306 treatment groups. These results demonstrate that H3.3-G34R pHGG cells are sensitive to IFNγ
307 stimulation and prone to IFNγ-induced apoptosis. To validate that this effect is conserved
308 regardless of the genetic background of the GEMM, we used a model that is independent of the
309 RAS pathway activation. In this model, we induced the tumors with short hairpins against *p53*
310 and *Atrx*, together with overexpression of a constitutively active mutant PDGFRα (D842V) in
311 CDKN2A KO animals. These alterations are common in G34-mutant pHGG. In this alternative
312 mouse CDKN2A KO/P53 KD driven model we found an increment in early apoptotic and
313 necrotic cells in G34R-mutant pHGG cells upon IFNγ stimulation (Figure S7). Additionally, we
314 assessed phosphorylated-STAT1 levels in this model in basal conditions and after IFNγ-
315 stimulation and found that STAT1 phosphorylation is significantly (p < 00001) increased in G34-
316 mutant tumors compared to their H3.3-Wt counterparts (Figure S6, C).

317 **JAK/STAT activation leads to MHC-I expression in G34R-mutant pHGG**

318 JAK/STAT signaling and CIITA activation were shown to activate MHC I expression, as CIITA is
319 a critical transcriptional regulator of the MHC class I and II complexes (Tur et al., 2021). MHC-I
320 expression on tumor cells can drive antitumor immunity via antigen presentation. We evaluated
321 CIITA and MHC-I levels in H3.3-Wt and H3.3-G34R pHGG mouse and human cells by western
322 blot. In line with ChIP-seq and RNA-seq results, we observed increased expression of these
323 proteins in G34-mutant mouse (Figure 4, B-D) and human (Figure S6, D-E) pHGG cells. We
324 confirmed these results by assessing MHC-I expression by flow cytometry in mouse and human
325 H3.3-Wt and H3.3-G34R pHGG cells, observing increased MHC-I expression in G34-mutant
326 pHGG cells (Figure 4, E-H). Furthermore, we compared the levels of MHC I genes in H3.3-G34-
327 mutant and H3.3-Wt pHGG cells by real-time PCR (qPCR). Our results indicate that the levels
328 of MHC class I genes are upregulated in H3.3-G34-mutant versus H3.3-Wt pHGG in our mouse
329 model (Figure S6, F).

330 **H3.3-G34R expression impacts on the immune cell infiltration into the glioma**
331 **microenvironment**

332 The molecular analysis of our H3.3-G34R GEMM indicates that there is an active crosstalk
333 between tumor cells and the immune cells in the TME. Thus, we analyzed the transcriptional
334 differences among immune cells (*i.e.*, CD45+ cells), purified from the H3.3-G34R and H3.3-Wt

335 pHGG models. At symptomatic stage, tumors were dissected from the mouse brain; a cell
336 suspension was prepared; and CD45+ cells were isolated from H3.3-G34R or H3.3-Wt pHGG
337 by magnetic sorting (Garcia-Fabiani et al., 2020a). Total RNA was purified from the CD45+ cells
338 and gene expression analysis was performed by RNA-Seq. The statistical analysis revealed 243
339 differentially expressed genes (adjusted p value < 0.05) in CD45+ cells purified from H3.3-G34R
340 tumors with respect to H3.3-Wt tumors (Figure 5, A; Supplementary Table 3). We observed that
341 genes related to the presence of T cells, such as *CD3g* and *CD3e* ($p<0.05$), and specifically to
342 cytotoxic CD8 T cells, such as *CD8a* and *CD8b1* ($p<0.05$ and $p<0.01$, respectively), were
343 significantly upregulated in immune cells from H3.3-G34R pHGG (Figure 5, A). On the contrary,
344 we found that the *CD34* marker ($p<0.01$), which is related to hematopoietic progenitor and stem
345 cells (Dmytrus et al., 2016), and genes associated with immunosuppression, such as *Arg1*
346 (Grzywa et al., 2020) ($p<0.05$), were downregulated in CD45+ cells derived from H3.3-G34R
347 pHGG when compared to CD45+ cells derived from H3.3-Wt pHGG (Figure 5, A-B), implying
348 that the immune cells of the H3.3-G34R pHGG TME are more differentiated and less
349 immunosuppressive than the immune cells from the H3.3-Wt TMEs.

350 Then, we performed a network analysis and clustering of the upregulated genes in H3.3-G34R-
351 derived CD45+ cells using the Reactome Functional Interaction plugin in Cytoscape (Shannon
352 et al., 2003). After network building and clustering, we detected 5 clusters with highly interacting
353 nodes (Figure 5, C-D). The analysis of the top-30 most significant pathways associated to these
354 clusters displayed terms that were related to immune system activation, especially to T cell-
355 mediated responses (Figure 5, C-D).

356 In summary, the transcriptional analysis of CD45+ cells isolated from the TME of H3.3-G34R
357 pHGG showed the upregulation of genes related to an activated T cell response.

358 To assess the immune cell infiltration pattern in H3.3-G34R pHGG and uncover how the
359 presence of the H3.3-G34R mutation affects the TME, we implanted H3.3-G34R or H3.3-Wt
360 cells in the brain of C57BL6 mice and, at symptomatic stage, pHGG were dissected and
361 processed for flow cytometry analysis (Figure 5, D). The analysis of T cell infiltration in the TME
362 of H3.3-Wt and H3.3-G34R pHGG is displayed in Figure 5, D- E. A significant increase in the
363 proportion of CD4 and CD8 T cell infiltrates were observed in H3.3-G34R pHGG TME ($p<0.001$)
364 (Figure 5, D). To further characterize CD4 T cells, we measured the expression of regulatory T
365 cells (Treg) markers CD25 and FoxP3. Tregs are essential cells for preventing autoimmunity
366 and for maintaining peripheral tolerance. However, they could also limit the anti-tumor immune
367 response (Vignali et al., 2008). Even though we observed an increase in the amount of CD4

368 Tregs in the TME of H3.3-G34R tumors compared to the amount of Tregs in the TME of H3.3-
369 Wt tumors (Figure 5, E), the ratio of CD8 T cells to Tregs was significantly higher in the H3.3-
370 G34R pHGG TME (Figure 5, E) ($p < 0.05$). To assess the role of T cells in G34-mutant pHGG
371 development, we compared the survival of C57BL/6, *Rag-1* KO (devoid of T and B-cells
372 (Mombaerts et al., 1992)), and Cd8 KO (devoid of Cd8+ T-cells) mice, implanted with H3.3-Wt
373 or H3.3-G34R pHGG cells. We observed a reduced survival of *Rag-1* KO (Figure S8, A, $p <$
374 0.05) and *Cd8* KO (Figure S8, B, $p<0.01$) mice that were implanted with H3.3-G34R cells, in
375 comparison to C57BL6. In the case of mice implanted with H3.3-Wt pHGG cells, there was no
376 survival difference between C57BL/6 and *Rag-1* KO; and the survival difference between
377 C57BL/6 and *Cd8* KO mice was only of 4 days ($p < 0.05$). The marked reduction in the MS
378 observed in mice bearing G34-mutant pHGG demonstrates the relevance of cytotoxic T cell
379 mediated anti-tumor activity in this model of pHGG. Additionally, we implanted the CDKN2A KO/
380 p53 KD/PDGFRA D842V/ATRX KD H3.3-Wt or H3.3G34R cells in NOD scid gamma (NSG)
381 mice. Our results show that in this immunocompromised host there is no difference in the MS
382 between H3.3-Wt and H3.3-G34R pHGG (Figure S8, C).

383 The tumor microenvironment (TME) of high-grade gliomas (HGG) is predominantly
384 immunosuppressive (McClellan et al., 2023) where immunosuppressive immune populations
385 potentially hinder the development of adaptive immunity responses. In this context, myeloid-
386 derived suppressor cells (MDSC), by limiting the function of T-cells, contribute to this
387 immunosuppressive state and prompt the reprogramming of T-cells towards regulatory or
388 exhausted phenotypes (Alban et al., 2018; Bayik et al., 2020; Gabrilovich et al., 2012; Gielen et
389 al., 2016; Kamran et al., 2018; Kamran et al., 2017; Mirghorbani et al., 2013). Particularly,
390 circulating and intra-tumoral density of MDSC positively correlates with the glioma grade, whilst
391 it negatively correlates with the patient's outcome (Alban et al., 2018).

392 To assess MDSC infiltration in the H3.3-G34R pHGG model, we implanted H3.3-G34R or H3.3-
393 Wt cells in the brain of C57BL6 mice and, at symptomatic stage, tumors were dissected and
394 processed for flow cytometry staining (Figure 6, A). The analysis of myeloid cells in the TME of
395 H3.3-G34R or H3.3-Wt pHGG revealed a reduced proportion of CD11b+ Gr-1+ cells (MDSC
396 general phenotype (Bronte et al., 2016)) in the H3.3-G34R pHGG ($p<0.0001$) (Figure 6, B-C).
397 MDSC phenotypic characterization also requires distinction between Monocytic (M) (CD45+
398 CD11b+ $Ly6C^{hi}$ $Ly6G^{-}$) MDSC and Polymorphonuclear (PMN) (CD45+ CD11b+ $Ly6C^{lo}$ $Ly6G^{+}$)
399 MDSC. We found similar proportions of cells displaying PMN-MDSC phenotype in the TME of
400 both tumors, but a significant decrease in the proportion of M-MDSCs in the TME of H3.3-G34R

401 pHGG ($p<0.01$) (Figure 6C-D). Similarly, we found less CD11b+ Gr-1+ cells in the TME of SB-
402 derived H3.3-G34R pHGG with respect to H3.3-Wt ($p<0.05$) (Figure S9, A, right panel). In this
403 model, M-MDSC and PMN-MDSC were found to be decreased in the TME of H3.3-G34R SB-
404 derived pHGG compared to their proportion in H3.3-Wt SB-derived HGG ($p<0.05$) (Figure S9, A,
405 left panel). Also, we assessed the expression of iNOS and ARG1, two proteins related to
406 immunosuppression (Bronte et al., 2016; Kamran et al., 2017; Mirghorbani et al., 2013), and
407 found no differences in their expression on cells with M-MDSC or PMN-MDSC phenotypes,
408 between H3.3-G34R and H3.3-Wt pHGG (Figure S9,C). The analysis of MDSC content in the
409 blood, bone marrow and spleen of H3.3-G34R or H3.3-Wt tumor bearing mice revealed no
410 differences in the proportion of M-MDSC or PMN-MDSC cells between the two groups (Figure
411 S9, D-E).

412 To further characterize the infiltration of myeloid cells in the TME of H3.3-Wt and H3.3-G34R
413 pHGG, we assessed the content of dendritic cells (DCs) and Macrophages (Figure 6, F-I). We
414 observed that H3.3-G34R TME was infiltrated with a higher proportion of DCs ($p<0.0001$)
415 (Figure 6, F-G) and total macrophages ($p<0.05$) (Figure 6, H-I), than the H3.3-Wt TME. Also, we
416 measured CD206 and MHCII expression on macrophages to classify them as anti-tumor M1
417 (CD45+ F4/80+ Ly6C- CD206- MHCII+) or pro-tumor M2 macrophages (CD45+ F4/80+ Ly6C-
418 CD206+ MHCII-) (Chen et al., 2019; Chen et al., 2017). Whilst the proportion of M2
419 macrophages to total macrophages was similar between H3.3-G34R and H3.3-Wt TMEs, M1
420 proportion was significantly increased in H3.3-G34R TME ($p<0.0001$) and the M1/M2 ratio was
421 higher in H3.3-G34R pHGG (Figure 6, J-L).

422 Taken together, the analysis of the TME revealed that H3.3-G34R pHGG are infiltrated with a
423 higher proportion of immune cells associated with the onset of an anti-tumor immune response.

424 **H3.3-G34R impacts the array of cytokines secreted by pHGG cells, rendering the TME**
425 **less immunosuppressive.**

426 Given that H3.3-G34R pHGG cells display a transcriptional landscape and a TME infiltration
427 pattern consistent with an activated immune response, analyzed how the presence of H3.3-
428 G34R alters the array of cytokines secreted by H3.3-G34R pHGG cells. We incubated $1x10^6$
429 H3.3-Wt or H3.3-G34R cells in T25 flasks and 48 hours later, the supernatants were analyzed
430 for cytokine concentration (Figure 7A). The secretion of G-CSF, VEGF, MCP-1, MCP-3, TGFβ
431 and N-Gal was lower in H3.3-G34R pHGG cells ($p<0.0001$). We investigated our ChIP-Seq data
432 to analyze the chromatin context of the genes encoding the differentially secreted cytokines. We

433 observed an increase in H3K27me3 (transcriptional repressive) mark deposition on the
434 promoter region of *CSF3* (gene that produces G-CSF) in H3.3-G34R pHGG cells with respect to
435 H3.3-Wt. On the contrary, H3K4me1, H3K4me and H3K27ac (transcriptional activation) marks
436 were found to be increased in the same region in H3.3-Wt vs H3.3-G34R pHGG cells (Figure 7,
437 B). These results indicate the presence of a permissive chromatin for G-CSF expression in
438 H3.3-Wt with respect to H3.3-G34R pHGG cells. We did not find differences in the deposition of
439 histone marks for the other cytokines with significantly different concentrations.

440 To assess the impact of the cytokines secreted by H3.3-G34R pHGG cells on T cell survival, we
441 performed T cell proliferation assays in the presence of conditioned media (CM) from H3.3-Wt
442 and H3.3-G34R pHGG cells (Figure 7, C). The addition of increasing amounts of H3.3-Wt CM
443 correlated with decreasing proportions of proliferating CD8 T cells ($p<0.0001$), whereas no
444 inhibition in CD8 T cell proliferation was observed in the presence of H3.3-G34R CM (Figure 7,
445 D-F). In accordance, IFNγ secretion decreased with the addition of increasing amounts of H3.3-
446 Wt CM, whereas IFNγ secretion increased with the addition of increasing amounts of H3.3-
447 G34R CM (Figure 7, G).

448 As we discovered these differences in cytokine secretion and their implications on T cell
449 proliferation, we analyzed the impact of H3.3-G34R or H3.3-Wt pHGG-derived factors in the
450 immunosuppressive functionality of CD11b+ Gr-1+ cells (MDCS phenotype) encountered in the
451 TME. To assess the immunosuppressive ability of the CD11b+ Gr-1+, we performed T cell
452 proliferation assay (Alghamri et al., 2020a). Immune cells with the phenotype CD11b+ Gr-1+
453 were sorted by flow cytometry from the TME of H3.3-G34R or H3.3-Wt tumors and co-cultured
454 with OT-I splenocytes labelled with CFSE; we added SIINFEKL; and, 96 hours later, we
455 measured CD8 T cell proliferation by CFSE dilution (Figure 7H). Whilst the CD11b+ Gr-1+ cells
456 from H3.3-Wt inhibited T cell proliferation by 50% ($p<0.0001$), CD11b+ Gr-1+ cells from H3.3-
457 G34R did not affect it (Figure 7I and 7J).

458 These data demonstrates that the presence of H3.3-G34R impacts the array of cytokines
459 secreted by tumor cells, creating a less immunosuppressive TME with respect to the H3.3-Wt
460 tumor cells. We observed that these secreted factors enable the proliferation of effector T cells
461 and do not induce the production of *bona fide* MDSC or their homing into the TME.

462 **TK/Flt3L immune-stimulatory gene therapy enhances anti-glioma immune response in**
463 **H3.3-G34R pHGG mouse model.**

464 As we observed an immune-permissive tumor microenvironment associated with the expression
465 of H3.3-G34R in the pHGG mouse model, we evaluated the efficacy of a cytotoxic immune-
466 stimulatory TK/Flt3L gene therapy (GT). This therapy entails injecting adenoviruses encoding
467 TK and Flt3L into the tumor, followed by ganciclovir (GCV) administration (Ali et al., 2005; Curtin
468 et al., 2009). The TK converts GCV into a competitive inhibitor of DNA synthesis, which leads to
469 tumor cell lysis and the concomitant release of tumor antigens (Curtin et al., 2009; Mendez et
470 al., 2020). Flt3L mediates DC recruitment and expansion in the TME, which uptake the tumor
471 antigens, traffic them to the draining lymph nodes and prime a robust anti-tumor cytotoxic and
472 memory T cell response, leading to tumor regression and long-term survival (Ali et al., 2005;
473 Curtin et al., 2009; Kamran et al., 2017; Mendez et al., 2020).

474 Thus, we treated H3.3-G34R pHGG-bearing animals with the TK/Flt3L GT or saline as depicted
475 in Figure 8, A. We observed a significant extension in the survival of animals harboring H3.3-
476 G34R gliomas treated with GT (MS=Not reached, $p < 0.001$), with respect to the control group
477 treated with saline (MS=44 DPI) (Figure 8, B-C). GT led to an effective cure rate of 60% (Figure
478 8, C). To assess the safety of this therapy, complete blood cell count and serum chemistry
479 analysis of H3.3-G34R pHGG-bearing mice treated with saline or GT was performed (Figure
480 S10, A). We did not find any differences in the amount of white blood cells (WBC) and red blood
481 cells (RBC); the percentage of hemoglobin; or in the hematocrit between the saline and GT
482 treated groups (Figure S10, A). Also, we observed that the levels of AST (Aspartate
483 transaminase) ALT (Alanine transaminase), Creatinin, and BUN (Blood urea nitrogen) were
484 within the normal range for mice treated with GT, indicating that the liver and the renal system
485 were functioning normally (Figure S10, B). The histological assessment of livers from animals
486 treated with saline or GT did not display any abnormalities (Figure S10, B). Additionally, IHC
487 analysis was performed to assess the brain anatomy on paraffin-embedded brain tissue from
488 saline or long-term survivors from gene therapy treated animals. Sections were stained for
489 Myelin Basic Protein (MBP) (myelin sheath marker, to assess neuronal structure), Glial fibrillary
490 acidic protein (GFAP) (Glial marker, to assess glial inflammation), Nestin (neural stem cell
491 marker which stains for tumors cells) and CD68 (monocytic lineage marker). The analysis
492 indicates that long term survivors have no signs of anatomical abnormalities or signs of tumor
493 growth (Figure S10, C).

494 As tumors remained undetectable by luminescence for more than 100 DPI in the GT-treated
495 long-term survivors, we rechallenged these animals in the contralateral hemisphere with H3.3-
496 G34R pHGG cells without further treatment to examine the development of immunological

memory. As controls, naïve animals were implanted with H3.3-G34R pHGG cells in the striatum. Most of long-term survivors from the GT experiment did not develop tumors after rechallenging at day 90 DPI, whereas those from the control group succumbed due to tumor burden (Figure 8, D). Rechallenged animals were euthanized at 90 DPI, perfused, and the brains were paraffin embedded and sectioned for histological analysis (Figure S10, C). After H&E staining, no tumor mass was detected in the rechallenged animals (Figure S10, C). Also, the histological assessment of the liver of these mice did not show any abnormalities (Figure S10, D). Additionally, serum metabolites were analyzed on the rechallenged animals, showing no alterations in any marker compared to the reference range (Figure S11), demonstrating that the gene therapy does not elicit toxic effects. These data demonstrates that TK/Flt3L GT is effective for the treatment of H3.3-G34R HGG and that it prompts the development of immunological memory.

To confirm the presence of anti-tumor specific CD8 T cells in the TME, we generated H3.3-G34R pHGG cells expressing the subrogate antigen ovalbumin (OVA). OVA antigen is a model protein for studying antigen-specific immune responses in mice (Alghamri et al., 2020b; Kamran et al., 2017; Mendez et al., 2020). H3.3-G34R-OVA cells were implanted in the striatum of C57BL/6 mice and at 14 DPI mice were treated with GT or saline, followed by treatment with GCV, twice a day for 7 days. Mice were euthanized at the end of GCV treatment and tumors were dissected to evaluate the immune response. The TME was examined to study the presence of total infiltrating T cells and anti-tumor specific CD8 T cells (Figure 8, E-G). Anti-tumor specific CD8 T cells were identified using SIINFEKL-H2K^{b}-Tetramer (Figure 8, G). We observed that the TME of animals treated with GT had a higher amount of CD45+ cells ($p<0.05$) (Figure 8, E) and CD3+ cells ($p<0.05$) (Figure 8, F) compared to the saline group TME. Moreover, GT-treated animals displayed an increased number of tumor-specific CD8 T cells (CD45+ CD3+ CD8+ Tetramer+) than the saline group ($p<0.01$) (Figure 8, G). In addition, we observed a decrease in exhausted T cells (CD45+ CD3+ TGIT+ TIM-3+) in the GT group compared to Saline animals ($p<0.05$) (Figure 8, H).

Collectively, these results demonstrate that the TK/Flt3L GT increases the amount of tumor-specific CD8 T cells in the TME of H3.3-G34R gliomas, enhancing the MS and contributing to the development of anti-tumor immunological memory.

DISCUSSION

529 The breakthroughs of the molecular characteristics associated with pediatric brain tumors have
530 led to the discovery that pHGG are intrinsically different from adult HGG, which could explain
531 why some of the therapies applied to adult brain tumors were not successful in the pediatric
532 population (Wang et al., 2019; Wu et al., 2014). Thus, to uncover therapeutic targets for pHGG
533 it is critical to understand the molecular features of these tumors.

534 We aimed to determine the biological features of a pHGG subtype that harbors a mutation in the
535 *H3F3A* gene, named H3.3-G34R. We used an immunocompetent genetically engineered mouse
536 model (GEMM) for this type of tumor that recapitulates the salient features of the human
537 disease (Haase et al., 2022). Previous work from our group demonstrated that G34-mutations
538 leads to impaired DNA damage responses and confers genomic instability (Haase et al., 2022).
539 We showed that DNA repair impairment leads to the activation of the cGAS/STING pathway in
540 G34R-mutant pHGG, activating the immune responses (Haase et al., 2022). In the present
541 work, we used an immunocompetent mouse model to better understand the tumor's molecular
542 characteristics and its immune microenvironment, and to test the effectiveness of an immune-
543 mediated gene therapeutic approach for H3.3-G34R pHGG.

544 The immune response in the brain differs from the immune response mounted in other parts of
545 the body due to anatomical particularities of the CNS (Engelhardt et al., 2017; Louveau et al.,
546 2015; Negi and Das, 2018; Ousman and Kubes, 2012; Ransohoff and Engelhardt, 2012).
547 Factors derived from neural cells promote quiescence and immunosuppression in the brain
548 microenvironment (Ousman and Kubes, 2012; Ransohoff and Engelhardt, 2012). Nevertheless,
549 in response to inflammatory stimuli, this quiescent immune state pivots, promoting the
550 proliferation of brain resident microglial cells, as well as increasing the permeability of the blood
551 brain barrier for the infiltration of myeloid cells and activated T cells (Mariani and Kielian, 2009;
552 Ousman and Kubes, 2012; Sampson et al., 2019; Weiss et al., 2016). Glioma TME has been
553 reported to be immunosuppressive (Antunes et al., 2020; Kamran et al., 2018; McClellan et al.,
554 2023; Quail and Joyce, 2017). It has been identified that myeloid cells are the major type of
555 immune cell in glioma's TME, with macrophages representing more than 30% of the tumor
556 mass (Chen et al., 2017; McClellan et al., 2023; Quail and Joyce, 2017). The TME analysis of
557 human samples revealed that intratumoral blood-derived macrophages display an
558 immunosuppressive transcriptional program and that their presence correlates with tumor
559 malignancy (Müller et al., 2017). Also, the hypoxic environment in glioma can induce the
560 infiltration of Tregs, which can suppress cytotoxic T cell activities, leading to tumor progression
561 (Deng, 2018; McClellan et al., 2023).

562 Whilst the majority of the studies related to glioma TME have been performed on adult patient
563 samples, the TME of pediatric brain tumors has remained understudied, hindering the
564 development of effective immune-mediated therapies. Using our immunocompetent H3.3-G34R
565 pHGG model, we were able to understand how the presence of this mutation impacts the
566 epigenomic and transcriptomic landscape of pHGG cells, affecting the tumor immune cell
567 infiltration. By RNA-Seq we observed that H3.3-G34R glioma cells had a transcriptional pattern
568 coherent with an active immune response in the TME. Specifically, we detected that H3.3-G34R
569 tumor cells were responding to IFNs, as several genes related to IFN-I (IFNα and IFNβ) and
570 IFN-II (IFNγ) signaling pathways were upregulated in H3.3-G34R pHGG cells with respect to
571 H3.3-Wt pHGG cells (Figure 1). We found the upregulation of genes that are downstream of the
572 IFNγ signaling pathway (*Irf1*, *Ciita* and genes related to MHC-I complex, (Figures 3 and 4)), in
573 H3.3-G34R pHGG cells (Schroder et al., 2004; Gocher et al., 2022; Muhlethaler-Mottet et al.,
574 1998). Moreover, we detected that several genes involved in IFNγ signaling displayed
575 transcriptionally permissive chromatin states (CS) in H3.3-G34R cells, in comparison to the
576 transcriptionally inactive or repressed CS observed for the same regions in H3.3-Wt (Figures 3
577 and 4), demonstrating that this transcriptional pattern is a consequence of the epigenetic
578 signature induced by H3.3-G34R. We also observed an overall postranslational activation of the
579 JAK/STAT signaling evidenced by phosphorylation arrays upon IFNγ-stimulation. This pathway
580 is widely conserved in mammals, and its activation impacts several biological processes,
581 including cell proliferation, differentiation, and apoptosis (Rawlings et al., 2004), and aberrant
582 activation of STAT proteins, particularly STAT1 and STAT5, has been described in glioma, and
583 their activation may be related to oncogenesis (Brantley and Benveniste, 2008; Swiatek-
584 Machado and Kaminska, 2020).

585 We observed that H3.3-G34R cells were more sensitive to this IFNγ stimulation, as they
586 displayed an increased pSTAT1/STAT1 and pSTAT5a/STAT5a ratios post-IFNγ treatment
587 (Figure 3, F-G and J). We also discovered that cells with the H3.3-G34R mutation exhibit an
588 increased susceptibility to apoptosis when treated with IFNγ compared to their H3.3-Wt
589 counterparts (Figure 3, L-M). The IFNγ-induced cell death in G34-mutant pHGG could
590 potentially facilitate an immunogenic mechanism, mediated through the release of Damage-
591 Associated Molecular Patterns (DAMPs) and cytokines.

592 The main sources of IFNγ are activated T cells, and also NK, B and antigen presenting cells
593 (Gocher et al., 2022). When we analyzed the transcriptome of tumor-infiltrating immune cells,
594 we found an upregulation of genes related to T cell presence/activation (Figure 5, A-C) and we

595 confirmed an increased T cell infiltration in the TME of H3.3-G34R tumors (Figure 5G). Also,
596 H3.3-G34R tumors had an increased CD8 T cells to T regs ratio (Figure 5, E). In this regard,
597 lower effector CD8/Treg ratios have been correlated to less favorable outcomes for cancer
598 patients (Baras et al.; deLeeuw et al., 2012). Our results indicate that H3.3-G34R TME is
599 infiltrated with IFNγ-secreting cells, which could be associated with the transcriptional activation
600 of IFNγ-regulated genes observed in H3.3-G34R pHGG tumor cells (Figure 2, B-E).

601 We observed a lower proportion of Gr-1+ CD11b+ cells (MDSC phenotype), an increased
602 proportion of DCs and macrophages, and an increased M1/M2 ratio in the TME of G34-mutant
603 pHGG with respect to the H3.3-Wt pHGG TME (Figure 6). In the clinical setting, it has been
604 observed that the quantity and activation status of MDSCs inversely correlates with patient
605 survival and that they can be a predictor of WHO tumor grade (Alban et al., 2020). PMN- and M-
606 MDSC can exert immunosuppression through different mechanisms and, as M-MDSC produce
607 high amounts of NO, ARG1 and immunosuppressive cytokines, they are known to have a higher
608 suppressive capacity than the PMN-MDSC, which produce factors with shorter half-life that
609 require close contact with the target cell (Gabrilovich et al., 2012; Kumar et al., 2016;
610 Mirghorbani et al., 2013; Kumar et al., 2016). In our pHGG GEMM, we found that the Gr-1+
611 CD11b+ cells isolated from H3.3-G34R TMEs were not immunosuppressive (Figure 7, H-J),
612 which revealed that H3.3-G34R tumors are not infiltrated with *bona fide* MDSC. On the other
613 hand, we found that H3.3-Wt TMEs had more M-MDSC (Figure 6C), which tend to be more
614 immunosuppressive (Kumar et al., 2016), and that these were effectively inhibitory (Figure 7, H-
615 J).

616 Is summary, our results showed that the TME of the H3.3-G34R pHGG is less
617 immunosuppressive than the TME of the control H3.3-Wt tumors. One explanation to these
618 observations could be related to the different array of cytokines secreted by H3.3-G34R or H3.3-
619 Wt cells (Figure 7, A), which could impact the immune cell infiltration or their effector activities.
620 One cytokine capable of inhibiting T cell proliferation, activation and effector functions is TGFβ
621 (Dahmani and Delisle, 2018; Thomas and Massagué, 2005). Specifically, TGFβ has been
622 shown to directly affect cytotoxic CD8 T cells' activity by inhibiting the expression of granzyme
623 A, granzyme B, perforin, Fas ligand and IFNγ, which are necessary for anti-tumor immunity
624 (Thomas and Massagué, 2005). Also, this cytokine induces the differentiation of Treg from
625 peripheral CD4 T cells, by inducing the expression of FoxP3 (Ghiringhelli et al., 2005; Oh and
626 Li, 2013) and has been detected in malignant glioma (Han et al., 2015). Thus, TGFβ secretion
627 by tumor cells promote neoplastic progression and tumor escape from the immune surveillance.

628 Our data shows that H3.3-G34R CM had significantly lower amounts of TGFβ compared to the
629 amounts found in the CM of H3.3-Wt cells (Figure 7, A). This correlates with the CD8 T cell
630 proliferation inhibition observed when OT-1 splenocytes were incubated with H3.3-WT CM
631 (Figure 7, E), but not when incubated with H3.3-G34R CM (Figure 7, F). Another effect
632 associated to TGFβ secretion is the induction of MDSC expansion, specifically M-MDSC (Lee et
633 al., 2018).

634 G-CSF is another cytokine that can be aberrantly secreted by cancer cells, stimulating MDSC
635 production by the bone marrow and increasing MDSC tumor infiltration (Bronte et al., 2016;
636 Gabrilovich et al., 2012; Li et al., 2016; Mirghorbani et al., 2013). Particularly, G-CSF has been
637 shown to be secreted by gliomas and the increase in G-CSF levels has been observed to
638 correlate with MDSC accumulation in glioblastoma patients (Alghamri et al., 2021; Aliper et al.,
639 2014; Kast et al., 2017; Raychaudhuri et al., 2011). G-CSF levels were also higher in H3.3-WT
640 CM with respect to H3.3-G34R CM. Accordingly, the histone mark deposition around the G-CSF
641 promoter region was indicative of transcriptional activation in H3.3-Wt pHGG cells (Figure 7, B).
642 Thus, the higher secretion of both TGFβ and G-CSF by H3.3-Wt pHGG cells correlates with a
643 higher MDSC infiltration in the H3.3-Wt TME with respect to the H3.3-G34R TME.

644 Thus, we could reason that the expression of the H3.3-G34R in pHGG cells is reshaping the
645 chromatin, affecting the transcriptome, and impacting on the type of cytokines being secreted by
646 these tumors, which would ultimately define the crosstalk between tumor and the immune
647 system as well as the TME infiltration pattern.

648 Although the microenvironment of H3.3-G34R pediatric high-grade glioma (pHGG) mouse
649 model is less immunosuppressive than that in H3.3-Wt pHGG, animals with H3.3-G34R tumors
650 still eventually succumb to tumor burden. In response, we examined the effectiveness of the
651 immune-boosting TK/Flt3L gene therapy (GT) (Figure 8A), a treatment our laboratory developed
652 that has recently completed a phase I clinical trial for adult HGG patients
653 (https://clinicaltrials.gov; identifier: NCT01811992) (Umemura et al., 2022; Ali et al., 2005;
654 Candolfi et al., 2012; Candolfi et al., 2014; Curtin et al., 2009; Kamran et al., 2017; Mendez et
655 al., 2020; Mineharu et al., 2012). Mice with H3.3-G34R pHGG that were treated with this
656 therapy lived longer than those receiving saline, and 60% became long-term survivors (Figure 8,
657 A-C). Furthermore, these survivors remained tumor-free even without additional treatment
658 Figure 8, D and S10, C). We also verified that this therapy increased the infiltration of CD45+
659 and pan T cells, thereby encouraging the growth and migration of tumor-specific CD8 T cells to
660 the brain (Figure 8, E-G). The presence of CD8 T cells is crucial for combatting cancer as they

661 can kill tumor cells and establish immunological memory (Murphy and Griffith, 2016), which is
662 particularly critical to prevent tumor recurrence after surgery. However, these T cells can
663 become exhausted and less responsive when continually exposed to antigens in non-ideal
664 conditions, as evidenced by the expression of certain co-inhibitory receptors. In human HGG
665 samples, these exhaustion markers are detectable on infiltrating T cells (Woroniecka and Fecci,
666 2018). In this study, we noticed decreased expression of these markers in CD8 T cells from GT-
667 treated animals (Figure 8, H). Overall, the TK/Flt3L GT therapy showed promise in this pre-
668 clinical H3.3-G34R pHGG model, prolonging survival and creating anti-tumor immunological
669 memory, while increasing the population of tumor-specific CD8 T cells and potentially delaying
670 or preventing T cell exhaustion.

671 In conclusion, our H3.3-G34R pHGG GEMM enabled us find for the first time that H3.3-G34R
672 presence affects the crosstalk between the HGG and the immune system. We demonstrated
673 that H3.3-G34R pHGGs are infiltrated with a pattern of immune cells that is consistent with an
674 anti-tumor response being mounted, which was found to be further enhanced by the application
675 of the TK/Flt3L GT. This immune stimulatory gene therapy (GT) increased the median survival
676 of H3.3-G34R tumor bearing animals and prompted the development of tumor-specific immune
677 response. Translationally, the pre-clinical data exhibited in this work represent robust evidence
678 to consider the TK/Flt3L as a feasible immune-mediated GT for the treatment of H3.3-G34R
679 malignant glioma patients. Additionally, our results suggest that G34R-mutant pHGG might
680 benefit from other immunotherapies such as CAR-T or PD-L1 therapies. This highlights the
681 relevance of the molecular stratification in the treatment decisions. To better understand the
682 tumor microenvironment (TME) of pediatric patients, more research is necessary, particularly to
683 elucidate the disparities attributable to various molecular subgroups. Most current research
684 involving patient samples primarily focuses on tumor cell analysis. However, associating
685 biological features with a specific molecular subgroup is challenging due to the scarcity of
686 suitable control tumors in patients. For example, there are few histone-Wild type pediatric high-
687 grade gliomas (pHGGs) that are hemispherical and possess a genetic background—specifically,
688 P53 knockout (KO) and ATRX knockout (KO)—comparable to that of G34R-mutant pHGGs. In
689 our study, we demonstrate a correlation between the findings from our mouse model and
690 transcriptomic data from patients, specifically noting an observed upregulation of the STAT
691 pathways in G34-mutant pHGG patients.

692 In summary, this study advances our knowledge of the intricate interplay between the H3.3-
693 G34R mutation, its impact on epigenomic and transcriptomic alterations, and the consequent

694 modulation of the tumor immune microenvironment. Our findings underscore a less
695 immunosuppressive tumor microenvironment in H3.3-G34R pHGGs, driven by the complex
696 interplay between molecular aberrations and ensuing immune responses. Additionally, our
697 investigation revealed the potential of TK/Flt3L gene therapy in increasing survival and fostering
698 an anti-tumor immune response, thereby providing robust preclinical evidence to consider this
699 approach for clinical translation in H3.3-G34R pHGG patients. As we continue to unveil the
700 mechanisms within pHGGs, it's clear that a better understanding of the tumor microenvironment
701 associated with various molecular subgroups is an area that demands further research.
702 Together, our findings set the stage for more personalized, effective therapeutic strategies,
703 highlighting the crucial role of molecular stratification in clinical decision-making for the
704 implementation of pHGG treatments.

705 **Author Contributions**

706 MBGF, SH, KB, BML, ZZ, AAM, XL, JL, PK, AT, FJN, MSA, AC, FMN, AJNC, BS, FMN and ME
707 performed experiments. MBGF, SH, KB, TQ, MAS, PRL, and MGC analyzed the data and
708 designed the figures. MBGF, SH, KB, PRL, MAS, and MGC designed the research and wrote
709 the manuscript. All authors were involved in editing the manuscript and provided final approval
710 of the manuscript.

711 **Declaration of Interests**

712 The authors declare no competing interests.

713 **ACKNOWLEDGMENTS**

714 The laboratories of MGC and PRL are supported by the National Institutes of Health
715 (NIH)/National Institute of Neurological Disorders and Stroke (NIH/NINDS) grants R37-
716 NS094804, R01-NS105556, R01-NS122536, R01-NS124167, and R21-NS123879-01, and
717 Rogel Cancer Center Scholar Award to M.G. Castro; NIH/NINDS grants R01-NS076991, R01-
718 NS082311, R01-NS096756, R01NS122234, and National Institutes of Health/National Cancer
719 Institute (NIH/NCI) R01-CA243916 to P.R. Lowenstein; the Department of Neurosurgery; and
720 The Pediatric Brain Tumor Foundation, Leah's Happy Hearts Foundation, Ian's Friends
721 Foundation (IFF), Chad Tough Foundation, Smiles for Sophie Forever Foundation to M.G.
722 Castro and P.R. Lowenstein; and the American Brain Tumor Association Basic Research
723 Fellowship ‘‘in Memory of Bruce and Brian Jackson’’ to M.B.G.F We would like to acknowledge
724 the University of Michigan Epigenomics Core, the Advance Genomics Core, the Flow Cytometry

Core, the In-Vivo Animal Core (IVAC) and the UMICH Single Cell Analysis Resource for providing services that contributed to this study.

755 **REFERENCES**

756 Alban, T. J., Alvarado, A. G., Sorensen, M. D., Bayik, D., Volovetz, J., Serbinowski, E., Mulkearns-Hubert,
757 E. E., Sinyuk, M., Hale, J. S., and Onzi, G. R. (2018). Global immune fingerprinting in glioblastoma patient
758 peripheral blood reveals immune-suppression signatures associated with prognosis. JCI insight *3*.
759 Alban, T. J., Bayik, D., Otvos, B., Rabljenovic, A., Leng, L., Jia-Shiun, L., Roversi, G., Lauko, A., Momin, A.
760 A., and Mohammadi, A. M. (2020). Glioblastoma myeloid-derived suppressor cell subsets express
761 differential macrophage migration inhibitory factor receptor profiles that can be targeted to reduce
762 immune suppression. Frontiers in immunology *11*, 1191.
763 Alghamri, M. S., Kamran, N., Kadiyala, P., Lowenstein, P. R., and Castro, M. G. (2020a). Functional assay
764 to assess T-cell inhibitory properties of myeloid derived suppressor cells (MDSCs) isolated from the
765 tumor microenvironment of murine glioma models. In Methods in Enzymology, (Elsevier), pp. 215-228.
766 Alghamri, M. S., McClellan, B. L., Avvari, R. P., Thalla, R., Carney, S., Hartlage, C. S., Haase, S., Ventosa,
767 M., Taher, A., Kamran, N.*, et al.* (2021). G-CSF secreted by mutant IDH1 glioma stem cells abolishes
768 myeloid cell immunosuppression and enhances the efficacy of immunotherapy. Sci Adv *7*, eabh3243.
769 Alghamri, M. S., Núñez, F. J., Kamran, N., Carney, S., Altshuler, D., Lowenstein, P. R., and Castro, M. G.
770 (2020b). Functional characterization of tumor antigen-specific T-cells isolated from the tumor
771 microenvironment of sleeping beauty induced murine glioma models. In Methods in Enzymology,
772 (Elsevier), pp. 91-106.
773 Ali, S., King, G. D., Curtin, J. F., Candolfi, M., Xiong, W., Liu, C., Puntel, M., Cheng, Q., Prieto, J., Ribas, A.*,*
774 *et al.* (2005). Combined immunostimulation and conditional cytotoxic gene therapy provide long-term
775 survival in a large glioma model. Cancer research *65*, 7194-7204.
776 Aliper, A. M., Frieden-Korovkina, V. P., Buzdin, A., Roumiantsev, S. A., and Zhavoronkov, A. (2014). A role
777 for G-CSF and GM-CSF in nonmyeloid cancers. Cancer medicine *3*, 737-746.
778 Antunes, A. R. P., Scheyltjens, I., Duerinck, J., Neyns, B., Movahedi, K., and Van Ginderachter, J. A.
779 (2020). Understanding the glioblastoma immune microenvironment as basis for the development of
780 new immunotherapeutic strategies. Elife *9*, e52176.
781 Bannister, A. J., and Kouzarides, T. (2011). Regulation of chromatin by histone modifications. Cell
782 research *21*, 381-395.
783 Baras, A., Drake, C., Liu, J., Gandhi, N., Kates, M., Hoque, M., Meeker, A., Hahn, N., Taube, J., and
784 Schoenberg, M. The ratio of CD8 to Treg tumor-infiltrating lymphocytes is associated with response to
785 cisplatin-based neoadjuvant chemotherapy in patients with muscle invasive urothelial carcinoma of the
786 bladder. Oncoimmunology. 2016; 5: e1134412. In.
787 Bayik, D., Zhou, Y., Park, C., Hong, C., Vail, D., Silver, D. J., Lauko, A., Roversi, G., Watson, D. C., and Lo, A.
788 (2020). Myeloid-derived suppressor cell subsets drive glioblastoma growth in a sex-specific manner.
789 Cancer Discovery.
790 Bjerke, L., Mackay, A., Nandhabalan, M., Burford, A., Jury, A., Popov, S., Bax, D. A., Carvalho, D., Taylor,
791 K. R., and Vinci, M. (2013). Histone H3. 3 mutations drive pediatric glioblastoma through upregulation of
792 MYCN. Cancer discovery *3*, 512-519.
793 Bogu, G. K., Vizán, P., Stanton, L. W., Beato, M., Di Croce, L., and Marti-Renom, M. A. (2016). Chromatin
794 and RNA maps reveal regulatory long noncoding RNAs in mouse. Molecular and cellular biology *36*, 809-
795 819.
796 Brantley, E. C., and Benveniste, E. N. (2008). Signal transducer and activator of transcription-3: a
797 molecular hub for signaling pathways in gliomas. Molecular Cancer Research *6*, 675-684.
798 Bronte, V., Brandau, S., Chen, S.-H., Colombo, M. P., Frey, A. B., Greten, T. F., Mandruzzato, S., Murray,
799 P. J., Ochoa, A., and Ostrand-Rosenberg, S. (2016). Recommendations for myeloid-derived suppressor
800 cell nomenclature and characterization standards. Nature communications *7*, 1-10.

801 Calinescu, A. A., Nunez, F. J., Koschmann, C., Kolb, B. L., Lowenstein, P. R., and Castro, M. G. (2015).
802 Transposon mediated integration of plasmid DNA into the subventricular zone of neonatal mice to
803 generate novel models of glioblastoma. J Vis Exp.
804 Candolfi, M., King, G. D., Yagiz, K., Curtin, J. F., Mineharu, Y., Muhammad, A. K., Foulad, D., Kroeger, K.
805 M., Barnett, N., Josien, R.*, et al.* (2012). Plasmacytoid dendritic cells in the tumor microenvironment:
806 immune targets for glioma therapeutics. Neoplasia (New York, NY) *14*, 757-770.
807 Candolfi, M., Yagiz, K., Wibowo, M., Ahlzadeh, G. E., Puntel, M., Ghiasi, H., Kamran, N., Paran, C.,
808 Lowenstein, P. R., and Castro, M. G. (2014). Temozolomide does not impair gene therapy-mediated
809 antitumor immunity in syngeneic brain tumor models. Clin Cancer Res *20*, 1555-1565.
810 Castro, F., Cardoso, A. P., Gonçalves, R. M., Serre, K., and Oliveira, M. J. (2018). Interferon-gamma at the
811 crossroads of tumor immune surveillance or evasion. Frontiers in immunology *9*, 847.
812 Chawla-Sarkar, M., Lindner, D. J., Liu, Y.-F., Williams, B., Sen, G. C., Silverman, R. H., and Borden, E. C.
813 (2003). Apoptosis and interferons: role of interferon-stimulated genes as mediators of apoptosis.
814 Apoptosis *8*, 237-249.
815 Chen, C. C. L., Deshmukh, S., Jessa, S., Hadjadj, D., Lisi, V., Andrade, A. F., Faury, D., Jawhar, W., Dali, R.,
816 Suzuki, H.*, et al.* (2020). Histone H3.3G34-Mutant Interneuron Progenitors Co-opt PDGFRA for
817 Gliomagenesis. Cell *183*, 1617-1633.e1622.
818 Chen, Y., Song, Y., Du, W., Gong, L., Chang, H., and Zou, Z. (2019). Tumor-associated macrophages: an
819 accomplice in solid tumor progression. Journal of biomedical science *26*, 1-13.
820 Chen, Z., Feng, X., Herting, C. J., Garcia, V. A., Nie, K., Pong, W. W., Rasmussen, R., Dwivedi, B., Seby, S.,
821 and Wolf, S. A. (2017). Cellular and molecular identity of tumor-associated macrophages in glioblastoma.
822 Cancer research *77*, 2266-2278.
823 Curtin, J. F., Liu, N., Candolfi, M., Xiong, W., Assi, H., Yagiz, K., Edwards, M. R., Michelsen, K. S., Kroeger,
824 K. M., Liu, C.*, et al.* (2009). HMGB1 mediates endogenous TLR2 activation and brain tumor regression.
825 PLoS medicine *6*, e10.
826 Dahmani, A., and Delisle, J.-S. (2018). TGF-β in T cell biology: implications for cancer immunotherapy.
827 Cancers *10*, 194.
828 deLeeuw, R. J., Kost, S. E., Kakal, J. A., and Nelson, B. H. (2012). The prognostic value of FoxP3+ tumor-
829 infiltrating lymphocytes in cancer: a critical review of the literature. Clinical cancer research *18*, 3022-
830 3029.
831 Deng, G. (2018). Tumor-infiltrating regulatory T cells: origins and features. American Journal of Clinical
832 and Experimental Immunology *7*, 81.
833 Dmytrus, J., Matthes-Martin, S., Pichler, H., Worel, N., Geyeregger, R., Frank, N., Frech, C., and Fritsch, G.
834 (2016). Multi-color immune-phenotyping of CD34 subsets reveals unexpected differences between
835 various stem cell sources. Bone marrow transplantation *51*, 1093-1100.
836 Engelhardt, B., Vajkoczy, P., and Weller, R. O. (2017). The movers and shapers in immune privilege of the
837 CNS. Nature immunology *18*, 123.
838 Fiziev, P., Akdemir, K. C., Miller, J. P., Keung, E. Z., Samant, N. S., Sharma, S., Natale, C. A., Terranova, C.
839 J., Maitituoheti, M., and Amin, S. B. (2017). Systematic epigenomic analysis reveals chromatin states
840 associated with melanoma progression. Cell reports *19*, 875-889.
841 Gabrilovich, D. I., Ostrand-Rosenberg, S., and Bronte, V. (2012). Coordinated regulation of myeloid cells
842 by tumours. Nature Reviews Immunology *12*, 253-268.
843 Garcia-Fabiani, M. B., Comba, A., Kadiyala, P., Haase, S., Núñez, F. J., Altshuler, D., Lowenstein, P. R., and
844 Castro, M. G. (2020a). Isolation and characterization of immune cells from the tumor microenvironment
845 of genetically engineered pediatric high-grade glioma models using the sleeping beauty transposon
846 system. In Methods in Enzymology, (Elsevier), pp. 369-388.

847 Garcia-Fabiani, M. B., Kadiyala, P., Lowenstein, P. R., and Castro, M. G. (2020b). An Optimized Protocol
848 for In Vivo Analysis of Tumor Cell Division in a Sleeping Beauty-Mediated Mouse Glioma Model. STAR
849 Protocols, 100044.
850 Ghiringhelli, F., Puig, P. E., Roux, S., Parcellier, A., Schmitt, E., Solary, E., Kroemer, G., Martin, F.,
851 Chauffert, B., and Zitvogel, L. (2005). Tumor cells convert immature myeloid dendritic cells into TGF-β–
852 secreting cells inducing CD4+ CD25+ regulatory T cell proliferation. The Journal of experimental
853 medicine *202*, 919-929.
854 Gianno, F., Antonelli, M., Ferretti, E., Massimino, M., Arcella, A., and Giangaspero, F. (2018). Pediatric
855 high-grade glioma: A heterogeneous group of neoplasms with different molecular drivers. Glioma *1*,
856 117.
857 Gielen, P. R., Schulte, B. M., Kers-Rebel, E. D., Verrijp, K., Bossman, S. A., Ter Laan, M., Wesseling, P., and
858 Adema, G. J. (2016). Elevated levels of polymorphonuclear myeloid-derived suppressor cells in patients
859 with glioblastoma highly express S100A8/9 and arginase and suppress T cell function. Neuro-oncology
860 *18*, 1253-1264.
861 Gocher, A. M., Workman, C. J., and Vignali, D. A. A. (2022). Interferon-γ: teammate or opponent in the
862 tumour microenvironment? Nat Rev Immunol *22*, 158-172.
863 Gonzalez Castro, L. N., Liu, I., and Filbin, M. (2023). Characterizing the biology of primary brain tumors
864 and their microenvironment via single-cell profiling methods. Neuro Oncol *25*, 234-247.
865 Griesinger, A. M., Birks, D. K., Donson, A. M., Amani, V., Hoffman, L. M., Waziri, A., Wang, M., Handler,
866 M. H., and Foreman, N. K. (2013). Characterization of distinct immunophenotypes across pediatric brain
867 tumor types. The Journal of Immunology *191*, 4880-4888.
868 Grzywa, T. M., Sosnowska, A., Matryba, P., Rydzynska, Z., Jasinski, M., Nowis, D., and Golab, J. (2020).
869 Myeloid Cell-Derived Arginase in Cancer Immune Response. Frontiers in Immunology *11*, 938.
870 Guerreiro Stucklin, A. S., Ryall, S., Fukuoka, K., Zapotocky, M., Lassaletta, A., Li, C., Bridge, T., Kim, B.,
871 Arnoldo, A., and Kowalski, P. E. (2019). Alterations in ALK/ROS1/NTRK/MET drive a group of infantile
872 hemispheric gliomas.
873 Haase, S., Banerjee, K., Mujeeb, A. A., Hartlage, C. S., Núñez, F. M., Núñez, F. J., Alghamri, M. S., Kadiyala,
874 P., Carney, S., Barissi, M. N.*, et al.* (2022). H3.3-G34 mutations impair DNA repair and promote
875 cGAS/STING-mediated immune responses in pediatric high-grade glioma models. J Clin Invest *132*.
876 Han, J., Alvarez-Breckenridge, C. A., Wang, Q.-E., and Yu, J. (2015). TGF-β signaling and its targeting for
877 glioma treatment. American journal of cancer research *5*, 945.
878 Hyun, K., Jeon, J., Park, K., and Kim, J. (2017). Writing, erasing and reading histone lysine methylations.
879 Experimental & molecular medicine *49*, e324-e324.
880 Jones, C., Karajannis, M. A., Jones, D. T. W., Kieran, M. W., Monje, M., Baker, S. J., Becher, O. J., Cho, Y.
881 J., Gupta, N., Hawkins, C.*, et al.* (2017). Pediatric high-grade glioma: biologically and clinically in need of
882 new thinking. Neuro Oncol *19*, 153-161.
883 Jorgovanovic, D., Song, M., Wang, L., and Zhang, Y. (2020). Roles of IFN-γ in tumor progression and
884 regression: a review. Biomarker Research *8*, 49.
885 Kamran, N., Chandran, M., Lowenstein, P. R., and Castro, M. G. (2018). Immature myeloid cells in the
886 tumor microenvironment: Implications for immunotherapy. Clinical Immunology *189*, 34-42.
887 Kamran, N., Kadiyala, P., Saxena, M., Candolfi, M., Li, Y., Moreno-Ayala, M. A., Raja, N., Shah, D.,
888 Lowenstein, P. R., and Castro, M. G. (2017). Immunosuppressive Myeloid Cells' Blockade in the Glioma
889 Microenvironment Enhances the Efficacy of Immune-Stimulatory Gene Therapy. Molecular therapy : the
890 journal of the American Society of Gene Therapy *25*, 232-248.
891 Kane, A., and Yang, I. (2010). Interferon-gamma in brain tumor immunotherapy. Neurosurgery Clinics *21*,
892 77-86.
893 Kast, R. E., Hill, Q. A., Wion, D., Mellstedt, H., Focosi, D., Karpel-Massler, G., Heiland, T., and Halatsch,
894 M.-E. (2017). Glioblastoma-synthesized G-CSF and GM-CSF contribute to growth and

895 immunosuppression: Potential therapeutic benefit from dapsone, fenofibrate, and ribavirin. Tumor
896 Biology *39*, 1010428317699797.
897 Khazaei, S., Chen, C. C. L., Andrade, A. F., Kabir, N., Azarafshar, P., Morcos, S. M., França, J. A., Lopes, M.,
898 Lund, P. J., Danieau, G.*, et al.* (2023). Single substitution in H3.3G34 alters DNMT3A recruitment to cause
899 progressive neurodegeneration. Cell *186*, 1162-1178.e1120.
900 Korshunov, A., Capper, D., Reuss, D., Schrimpf, D., Ryzhova, M., Hovestadt, V., Sturm, D., Meyer, J.,
901 Jones, C., and Zheludkova, O. (2016). Histologically distinct neuroepithelial tumors with histone 3 G34
902 mutation are molecularly similar and comprise a single nosologic entity. Acta neuropathologica *131*,
903 137-146.
904 Koschmann, C., Calinescu, A. A., Nunez, F. J., Mackay, A., Fazal-Salom, J., Thomas, D., Mendez, F.,
905 Kamran, N., Dzaman, M., Mulpuri, L.*, et al.* (2016a). ATRX loss promotes tumor growth and impairs
906 nonhomologous end joining DNA repair in glioma. Sci Transl Med *8*, 328ra328.
907 Koschmann, C., Zamler, D., MacKay, A., Robinson, D., Wu, Y.-M., Doherty, R., Marini, B., Tran, D., Garton,
908 H., and Muraszko, K. (2016b). Characterizing and targeting PDGFRA alterations in pediatric high-grade
909 glioma. Oncotarget *7*, 65696.
910 Kumar, V., Patel, S., Tcyganov, E., and Gabrilovich, D. I. (2016). The nature of myeloid-derived suppressor
911 cells in the tumor microenvironment. Trends in immunology *37*, 208-220.
912 Lee, C.-R., Lee, W., Cho, S. K., and Park, S.-G. (2018). Characterization of multiple cytokine combinations
913 and TGF-β on differentiation and functions of myeloid-derived suppressor cells. International journal of
914 molecular sciences *19*, 869.
915 Lewis, P. W., Müller, M. M., Koletsky, M. S., Cordero, F., Lin, S., Banaszynski, L. A., Garcia, B. A., Muir, T.
916 W., Becher, O. J., and Allis, C. D. (2013). Inhibition of PRC2 activity by a gain-of-function H3 mutation
917 found in pediatric glioblastoma. Science *340*, 857-861.
918 Li, W., Zhang, X., Chen, Y., Xie, Y., Liu, J., Feng, Q., Wang, Y., Yuan, W., and Ma, J. (2016). G-CSF is a key
919 modulator of MDSC and could be a potential therapeutic target in colitis-associated colorectal cancers.
920 Protein & cell *7*, 130-140.
921 Lin, G. L., Wilson, K. M., Ceribelli, M., Stanton, B. Z., Woo, P. J., Kreimer, S., Qin, E. Y., Zhang, X., Lennon,
922 J., and Nagaraja, S. (2019). Therapeutic strategies for diffuse midline glioma from high-throughput
923 combination drug screening. Science translational medicine *11*.
924 Louveau, A., Smirnov, I., Keyes, T. J., Eccles, J. D., Rouhani, S. J., Peske, J. D., Derecki, N. C., Castle, D.,
925 Mandell, J. W., and Lee, K. S. (2015). Structural and functional features of central nervous system
926 lymphatic vessels. Nature *523*, 337-341.
927 Mackay, A., Burford, A., Carvalho, D., Izquierdo, E., Fazal-Salom, J., Taylor, K. R., Bjerke, L., Clarke, M.,
928 Vinci, M., Nandhabalan, M.*, et al.* (2017). Integrated Molecular Meta-Analysis of 1,000 Pediatric High-
929 Grade and Diffuse Intrinsic Pontine Glioma. Cancer Cell *32*, 520-537.e525.
930 Mackay, A., Burford, A., Molinari, V., Jones, D. T. W., Izquierdo, E., Brouwer-Visser, J., Giangaspero, F.,
931 Haberler, C., Pietsch, T., Jacques, T. S.*, et al.* (2018). Molecular, Pathological, Radiological, and Immune
932 Profiling of Non-brainstem Pediatric High-Grade Glioma from the HERBY Phase II Randomized Trial.
933 Cancer Cell *33*, 829-842.e825.
934 Mariani, M. M., and Kielian, T. (2009). Microglia in infectious diseases of the central nervous system.
935 Journal of Neuroimmune Pharmacology *4*, 448-461.
936 McClellan, B. L., Haase, S., Nunez, F. J., Alghamri, M. S., Dabaja, A. A., Lowenstein, P. R., and Castro, M.
937 G. (2023). Impact of epigenetic reprogramming on antitumor immune responses in glioma. The Journal
938 of Clinical Investigation *133*.
939 Mendez, F., Kadiyala, P., Nunez, F. J., Carney, S., Nunez, F. M., Gauss, J. C., Ravindran, R., Pawar, S.,
940 Edwards, M., and Garcia-Fabiani, M. B. (2020). Therapeutic efficacy of immune stimulatory thymidine
941 kinase and fms-like tyrosine kinase 3 ligand (TK/Flt3L) gene therapy in a mouse model of high grade
942 brainstem glioma. Clinical Cancer Research.

943 Miklja, Z., Pasternak, A., Stallard, S., Nicolaides, T., Kline-Nunnally, C., Cole, B., Beroukhim, R.,
944 Bandopadhayay, P., Chi, S., and Ramkissoon, S. H. (2019). Molecular profiling and targeted therapy in
945 pediatric gliomas: review and consensus recommendations. Neuro-oncology *21*, 968-980.
946 Mineharu, Y., Muhammad, A. K., Yagiz, K., Candolfi, M., Kroeger, K. M., Xiong, W., Puntel, M., Liu, C.,
947 Levy, E., Lugo, C.*, et al.* (2012). Gene therapy-mediated reprogramming tumor infiltrating T cells using IL-
948 2 and inhibiting NF-kappaB signaling improves the efficacy of immunotherapy in a brain cancer model.
949 Neurotherapeutics : the journal of the American Society for Experimental NeuroTherapeutics *9*, 827-
950 843.
951 Mirghorbani, M., Van Gool, S., and Rezaei, N. (2013). Myeloid-derived suppressor cells in glioma. Expert
952 review of neurotherapeutics *13*, 1395-1406.
953 Mombaerts, P., Iacomini, J., Johnson, R. S., Herrup, K., Tonegawa, S., and Papaioannou, V. E. (1992).
954 RAG-1-deficient mice have no mature B and T lymphocytes. Cell *68*, 869-877.
955 Muhlethaler-Mottet, A., Di Berardino, W., Otten, L. A., and Mach, B. (1998). Activation of the MHC class
956 II transactivator CIITA by interferon-γ requires cooperative interaction between Stat1 and USF-1.
957 Immunity *8*, 157-166.
958 Müller, S., Kohanbash, G., Liu, S. J., Alvarado, B., Carrera, D., Bhaduri, A., Watchmaker, P. B., Yagnik, G.,
959 Di Lullo, E., and Malatesta, M. (2017). Single-cell profiling of human gliomas reveals macrophage
960 ontogeny as a basis for regional differences in macrophage activation in the tumor microenvironment.
961 Genome biology *18*, 234.
962 Murphy, K. A., and Griffith, T. S. (2016). CD8 T Cell–Independent Antitumor Response and Its Potential
963 for Treatment of Malignant Gliomas. Cancers *8*, 71.
964 Negi, N., and Das, B. K. (2018). CNS: Not an immunoprivilaged site anymore but a virtual secondary
965 lymphoid organ. International reviews of immunology *37*, 57-68.
966 Ney, G. M., McKay, L. M., Koschmann, C., Mody, R., and Li, Q. (2020). The Emerging Role of Ras Pathway
967 Signaling in Pediatric Cancer. Cancer Research.
968 Núñez, F. J., Mendez, F. M., Kadiyala, P., Alghamri, M. S., Savelieff, M. G., Garcia-Fabiani, M. B., Haase,
969 S., Koschmann, C., Calinescu, A.-A., Kamran, N.*, et al.* (2019). IDH1-R132H acts as a tumor suppressor in
970 glioma via epigenetic up-regulation of the DNA damage response. Science translational medicine *11*,
971 eaaq1427.
972 Oh, S. A., and Li, M. O. (2013). TGF-β: guardian of T cell function. The Journal of Immunology *191*, 3973-
973 3979.
974 Ostrom, Q. T., Cioffi, G., Gittleman, H., Patil, N., Waite, K., Kruchko, C., and Barnholtz-Sloan, J. S. (2019).
975 CBTRUS statistical report: primary brain and other central nervous system tumors diagnosed in the
976 United States in 2012–2016. Neuro-oncology *21*, v1-v100.
977 Ousman, S. S., and Kubes, P. (2012). Immune surveillance in the central nervous system. Nature
978 neuroscience *15*, 1096-1101.
979 Pathak, P., Jha, P., Purkait, S., Sharma, V., Suri, V., Sharma, M. C., Faruq, M., Suri, A., and Sarkar, C.
980 (2015). Altered global histone-trimethylation code and H3F3A-ATRX mutation in pediatric GBM. Journal
981 of neuro-oncology *121*, 489-497.
982 Paugh, B. S., Qu, C., Jones, C., Liu, Z., Adamowicz-Brice, M., Zhang, J., Bax, D. A., Coyle, B., Barrow, J.,
983 Hargrave, D.*, et al.* (2010). Integrated molecular genetic profiling of pediatric high-grade gliomas reveals
984 key differences with the adult disease. Journal of clinical oncology : official journal of the American
985 Society of Clinical Oncology *28*, 3061-3068.
986 Plant, A. S., Koyama, S., Sinai, C., Solomon, I. H., Griffin, G. K., Ligon, K. L., Bandopadhayay, P., Betensky,
987 R., Emerson, R., and Dranoff, G. (2018). Immunophenotyping of pediatric brain tumors: correlating
988 immune infiltrate with histology, mutational load, and survival and assessing clonal T cell response.
989 Journal of neuro-oncology *137*, 269-278.

990 Puntonet, J., Dangouloff-Ros, V., Saffroy, R., Pagès, M., Andreiuolo, F., Grill, J., Puget, S., Boddaert, N.,
991 and Varlet, P. (2018). Historadiological correlations in high-grade glioma with the histone 3.3 G34R
992 mutation. Journal of Neuroradiology *45*, 316-322.
993 Quail, D. F., and Joyce, J. A. (2017). The microenvironmental landscape of brain tumors. Cancer cell *31*,
994 326-341.
995 Ransohoff, R. M., and Engelhardt, B. (2012). The anatomical and cellular basis of immune surveillance in
996 the central nervous system. Nature Reviews Immunology *12*, 623-635.
997 Rawlings, J. S., Rosler, K. M., and Harrison, D. A. (2004). The JAK/STAT signaling pathway. Journal of cell
998 science *117*, 1281-1283.
999 Raychaudhuri, B., Rayman, P., Ireland, J., Ko, J., Rini, B., Borden, E. C., Garcia, J., Vogelbaum, M. A., and
1000 Finke, J. (2011). Myeloid-derived suppressor cell accumulation and function in patients with newly
1001 diagnosed glioblastoma. Neuro-oncology *13*, 591-599.
1002 Sampson, J. H., Gunn, M. D., Fecci, P. E., and Ashley, D. M. (2019). Brain immunology and
1003 immunotherapy in brain tumours. Nature Reviews Cancer, 1-14.
1004 Schroder, K., Hertzog, P. J., Ravasi, T., and Hume, D. A. (2004). Interferon-γ: an overview of signals,
1005 mechanisms and functions. Journal of leukocyte biology *75*, 163-189.
1006 Schwartzentruber, J., Korshunov, A., Liu, X.-Y., Jones, D. T., Pfaff, E., Jacob, K., Sturm, D., Fontebasso, A.
1007 M., Quang, D.-A. K., and Tönjes, M. (2012). Driver mutations in histone H3. 3 and chromatin remodelling
1008 genes in paediatric glioblastoma. Nature *482*, 226-231.
1009 Shannon, P., Markiel, A., Ozier, O., Baliga, N. S., Wang, J. T., Ramage, D., Amin, N., Schwikowski, B., and
1010 Ideker, T. (2003). Cytoscape: a software environment for integrated models of biomolecular interaction
1011 networks. Genome Res *13*, 2498-2504.
1012 Siegel, R. L., Miller, K. D., and Jemal, A. (2016). Cancer statistics, 2016. CA: a cancer journal for clinicians
1013 *66*, 7-30.
1014 Sturm, D., Witt, H., Hovestadt, V., Khuong-Quang, D.-A., Jones, D. T., Konermann, C., Pfaff, E., Tönjes, M.,
1015 Sill, M., and Bender, S. (2012a). Hotspot mutations in H3F3A and IDH1 define distinct epigenetic and
1016 biological subgroups of glioblastoma. Cancer cell *22*, 425-437.
1017 Sturm, D., Witt, H., Hovestadt, V., Khuong-Quang, D. A., Jones, D. T., Konermann, C., Pfaff, E., Tonjes, M.,
1018 Sill, M., Bender, S.*, et al.* (2012b). Hotspot mutations in H3F3A and IDH1 define distinct epigenetic and
1019 biological subgroups of glioblastoma. Cancer Cell *22*, 425-437.
1020 Swiatek-Machado, K., and Kaminska, B. (2020). STAT signaling in glioma cells. In Glioma Signaling,
1021 (Springer), pp. 203-222.
1022 Thomas, D. A., and Massagué, J. (2005). TGF-β directly targets cytotoxic T cell functions during tumor
1023 evasion of immune surveillance. Cancer cell *8*, 369-380.
1024 Tur, J., Farrera, C., Sánchez-Tilló, E., Vico, T., Guerrero-Gonzalez, P., Fernandez-Elorduy, A., Lloberas, J.,
1025 and Celada, A. (2021). Induction of CIITA by IFN-γ in macrophages involves STAT1 activation by JAK and
1026 JNK. Immunobiology *226*, 152114.
1027 Umemura, Y., Orringer, D., Junck, L., Heth, J., Sagher, O., Leung, D., Mammoser, A., Hervey-Jumper, S.,
1028 Varela, M. L., Comba, A.*, et al.* (2022). Combined Cytotoxic and Immune Therapy for Primary Adult High-
1029 Grade Glioma. medRxiv, 2022.2011.2004.22281950.
1030 Vignali, D. A., Collison, L. W., and Workman, C. J. (2008). How regulatory T cells work. Nature Reviews
1031 Immunology *8*, 523-532.
1032 Wang, S. S., Bandopadhayay, P., and Jenkins, M. R. (2019). Towards immunotherapy for pediatric brain
1033 tumors. Trends in immunology *40*, 748-761.
1034 Weiss, T., Weller, M., and Roth, P. (2016). Immunological effects of chemotherapy and radiotherapy
1035 against brain tumors. Expert review of anticancer therapy *16*, 1087-1094.

1036 Wiesner, S. M., Decker, S. A., Larson, J. D., Ericson, K., Forster, C., Gallardo, J. L., Long, C., Demorest, Z. L.,
1037 Zamora, E. A., Low, W. C*., et al.* (2009). De novo induction of genetically engineered brain tumors in
1038 mice using plasmid DNA. Cancer Res *69*, 431-439.
1039 Woroniecka, K., and Fecci, P. E. (2018). T-cell exhaustion in glioblastoma. Oncotarget *9*, 35287.
1040 Wu, G., Broniscer, A., McEachron, T. A., Lu, C., Paugh, B. S., Becksfort, J., Qu, C., Ding, L., Huether, R., and
1041 Parker, M. (2012). Somatic histone H3 alterations in pediatric diffuse intrinsic pontine gliomas and non-
1042 brainstem glioblastomas. Nature genetics *44*, 251.
1043 Wu, G., Diaz, A. K., Paugh, B. S., Rankin, S. L., Ju, B., Li, Y., Zhu, X., Qu, C., Chen, X., and Zhang, J. (2014).
1044 The genomic landscape of diffuse intrinsic pontine glioma and pediatric non-brainstem high-grade
1045 glioma. Nature genetics *46*, 444.
1046 Yoshimoto, K., Hatae, R., Sangatsuda, Y., Suzuki, S. O., Hata, N., Akagi, Y., Kuga, D., Hideki, M., Yamashita,
1047 K., and Togao, O. (2017). Prevalence and clinicopathological features of H3. 3 G34-mutant high-grade
1048 gliomas: a retrospective study of 411 consecutive glioma cases in a single institution. Brain tumor
1049 pathology *34*, 103-112.

1050

1051

1052

1053

1054

1055

1056

1057

1058

1059

1060

1061

1062

1063

1064

1065

1066

1067

1068

1069

Figure 1 - Transcriptome analysis of mouse pHGG cells and patients' datasets

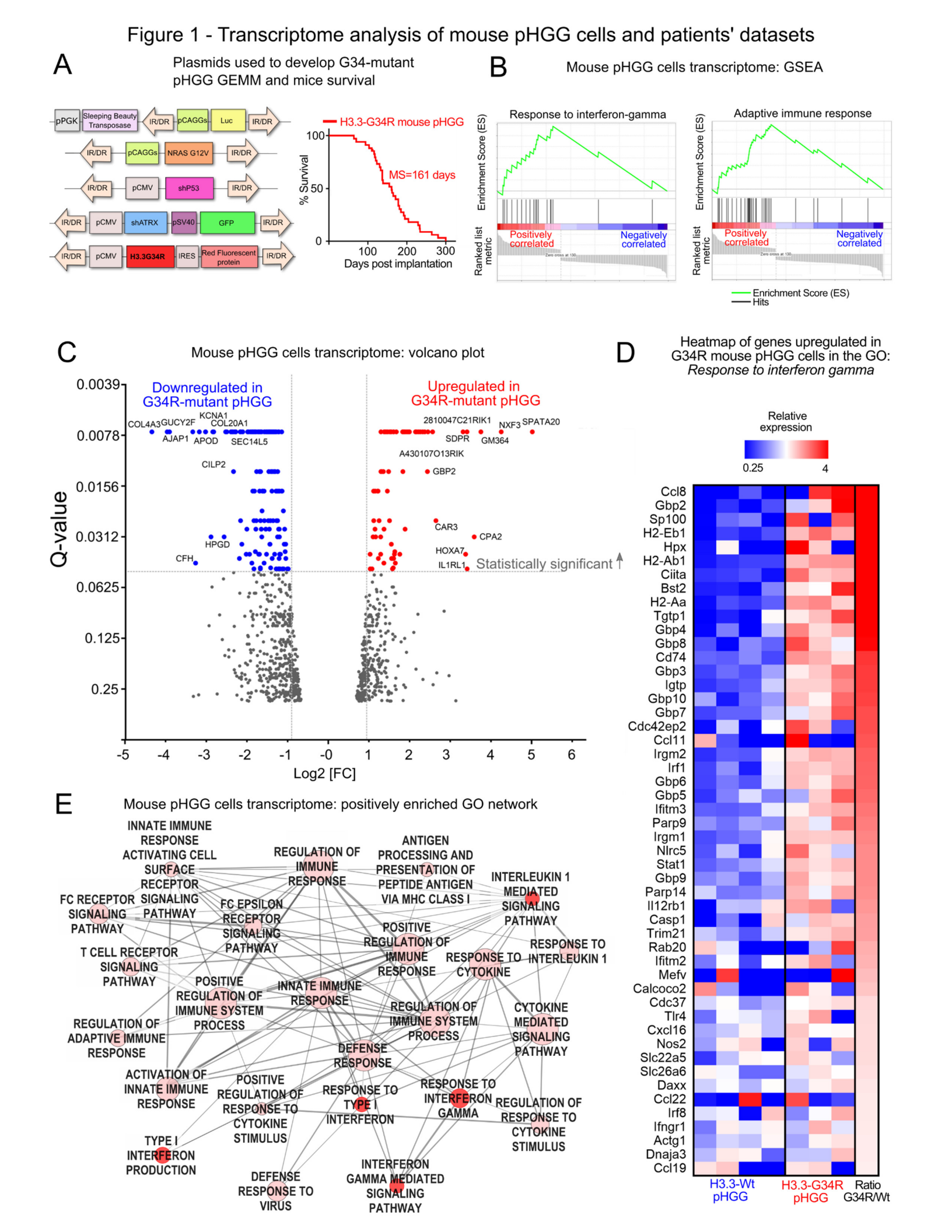

1098 **Figure 1. Transcriptomics analysis of mouse pHGG and patients' data. A)**
1099 Illustration of the transposable plasmids utilized to induce H3.3-Wt and H3.3-G34R
1100 pHGG in mice; and Kaplan-Meier survival curve for SB-derived H3.3-G34R (n=34)
1101 tumor bearing animals. **B)** Gene set enrichment analysis (GSEA) showing the
1102 upregulation of interferon-gamma and adaptive immune pathways in mouse H3.3-G34R
1103 versus H3.3-Wt pHGG tumor cells. **C)** Volcano plot depicting the transcriptional
1104 differences between mouse H3.3-G34R and H3.3-Wt pHGG tumor cells. **D)** Heatmap of
1105 genes belonging to the GO "*Response to interferon gamma*" upregulated in mouse
1106 H3.3-G34R versus H3.3-Wt pHGG tumor cells. **E)** Network of selected gene ontologies
1107 (GO) upregulated in pathways in mouse H3.3-G34R versus H3.3-Wt pHGG tumor cells.

1108

1109

1110

1111

1112

1113

1114

1115

1116

1117

Figure 2 - Characterization of the G34R pHGG epigenome by ChIP-seq

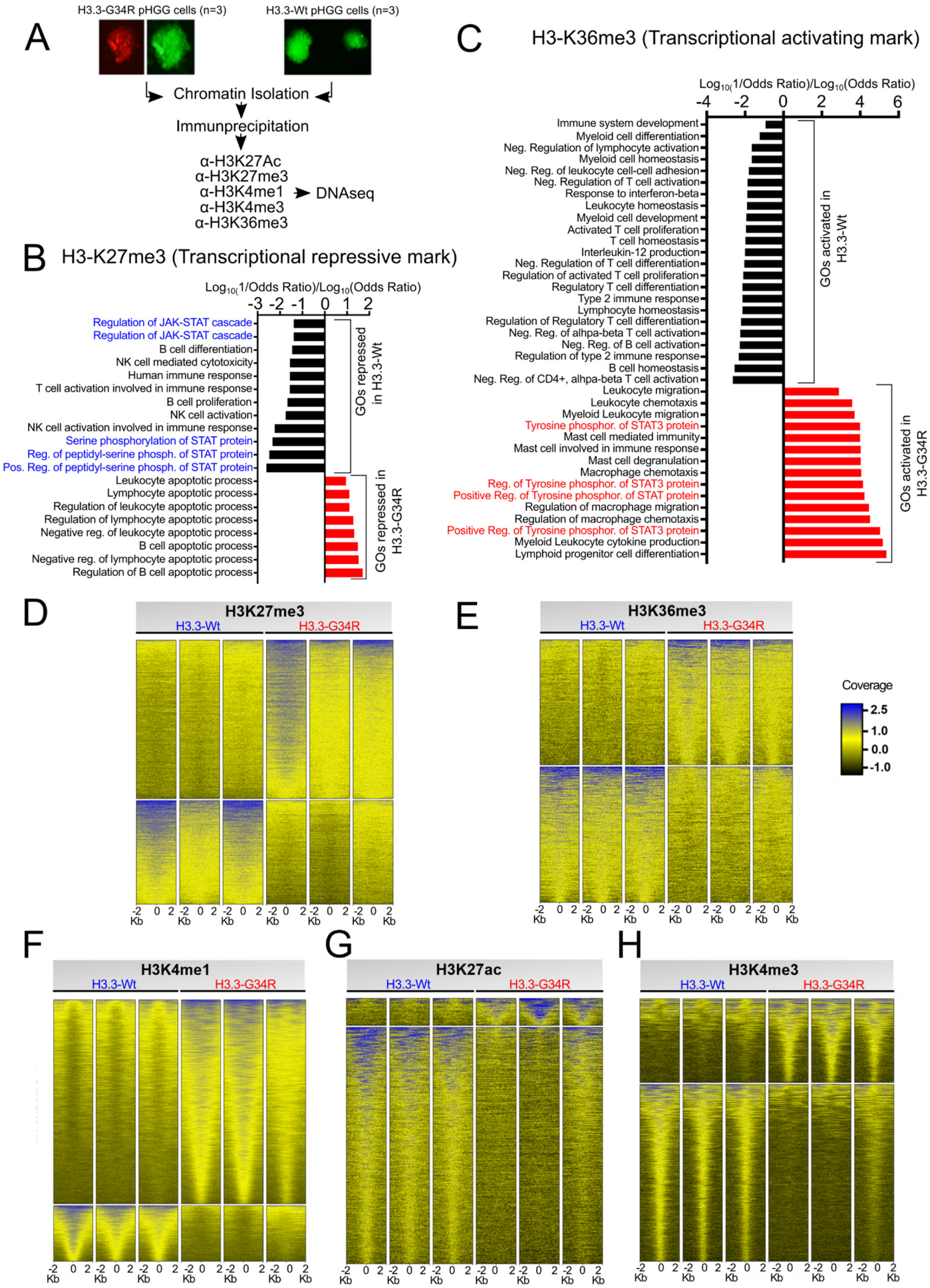

1136 **Figure 2. Characterization of the G34R pHGG epigenome by ChIP-seq. A)**
1137 Experimental outline for the ChIP-Sequencing analysis. Three biological replicates of
1138 H3.3-WT and H3.3-G34R neurospheres (NS) were used to perform the ChIP-Seq. Five
1139 marks were analyzed: H3K27ac, H3K27me3, H3K4me1, H3K4me3 and H3K36me3. **B-**
1140 **C)** Analysis of differentially enriched peaks for H3K27me3 **(B)** (transcriptional
1141 repression) or H3K36me3 **(C)** (transcriptional activation) histone marks revealed genes
1142 that are linked to distinct functional GO terms. GO enriched in the marks in H3.3-G34R
1143 versus H3.3-Wt pHGG are indicated with red bars and GO enriched in the marks in
1144 H3.3-Wt versus H3.3-G34R pHGG are indicated with black bars. The JAK/STAT related
1145 GO epigenetically active in H3.3-G34R cells (as indicated by enrichment of K36me3)
1146 are highlighted in red, and the same GO epigenetically downregulated in H3.3-Wt cells
1147 are highlighted in blue. **D-H)** Heat maps showing **D)** H3K27me3, **E)** H3K36me3, **F)**
1148 H3K4me1, **G)** H3K27ac and **H)** H3K4me3 differential peaks ± 2 kilo–base (Kb) pair from
1149 the gene center. Each row represents a distinct gene. The blue-to-yellow color gradient
1150 indicates high-to-low counts in the corresponding regions. The heat maps were
1151 generated from n=3 biological replicates per tumor type.

1152

1153

1154

1155

1156

1157

Figure 3 - Epigenetic activation of the STAT pathway in H3.3-G34 pHGG

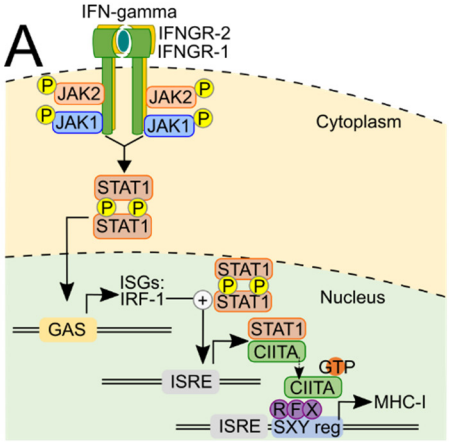

B

Gene	H3.3-Wt	H3.3-G34R
Stat1	Quiescent/Low (S13)	Flanking TSS Downstream (S3)
Stat5b	Quiescent/Low/Genic enhancer1/ Genic enhancer/Strong transcription	Flanking Tss Upstream 1/ Active Enhancer
Sp100	Quiescent/Low (S13)	Flanking TSS Downstream (S3)
H2-Eb1	Repressed Polycomb (S12)	Bivalent/Poised TSS (S2)
H2-Ab1	Repressed Polycomb (S12)	Bivalent/Poised TSS (S2)
H2-Aa	Repressed Polycomb (S12)	Bivalent/Poised TSS (S2)
Ciita	Repressed Polycomb (S12)	Bivalent/Poised TSS (S2)
Igtp	Repressed Polycomb (S12)	Flanking TSS Upsteam 2 (S4)

C

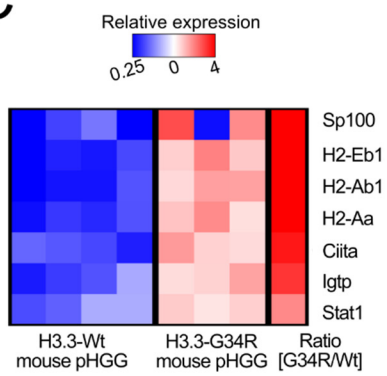

D

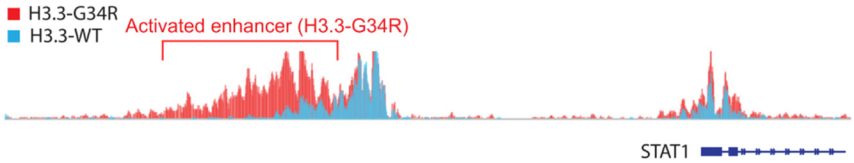

E

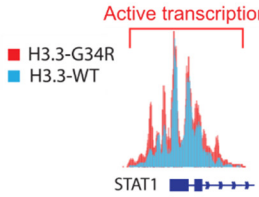

F

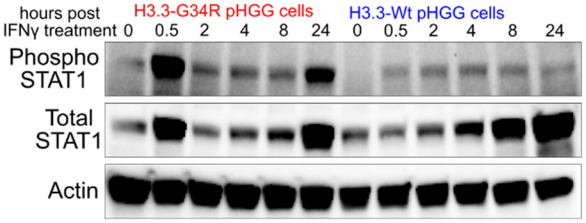

G

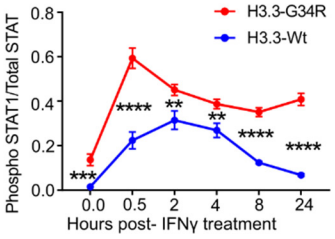

H

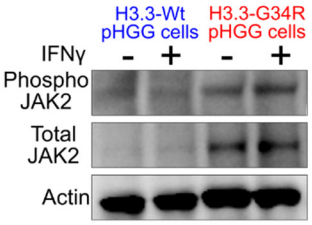

I

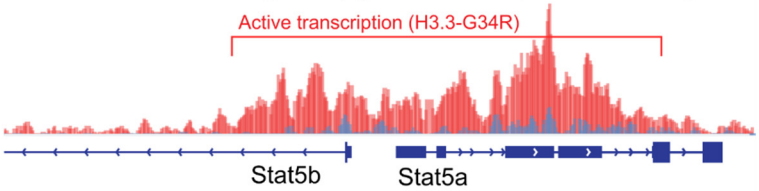

J

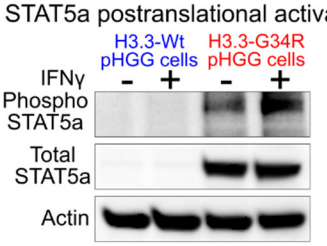

K

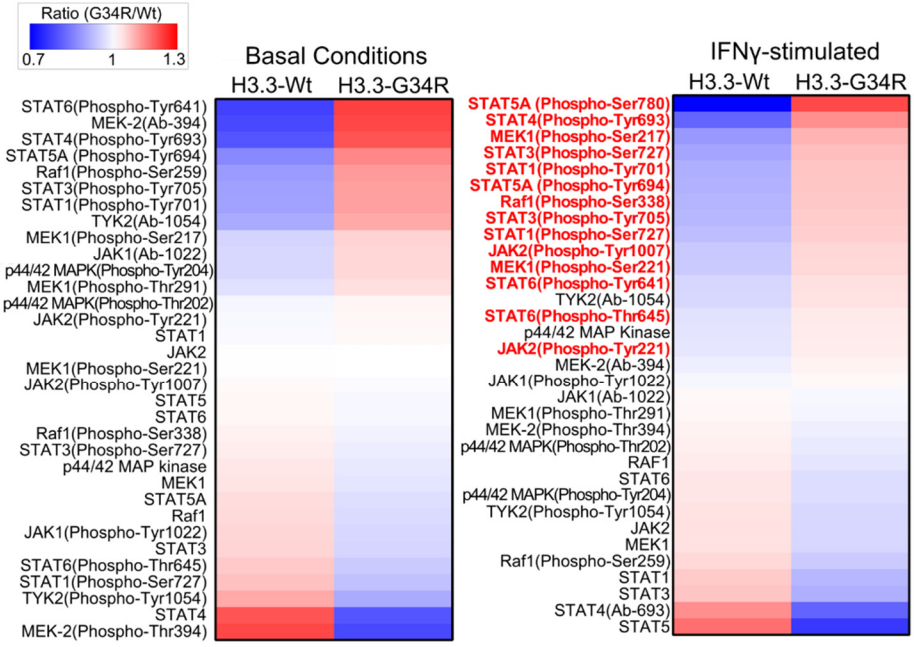

L

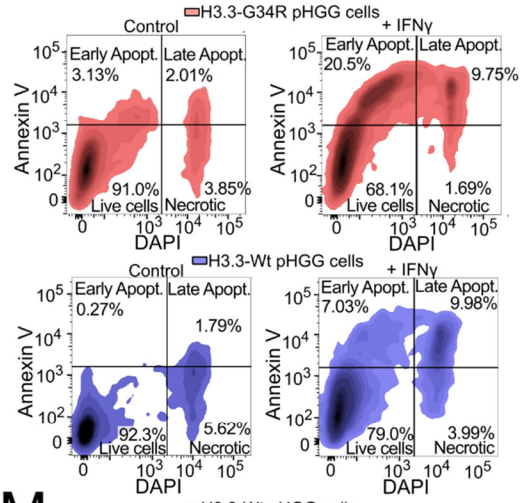

M

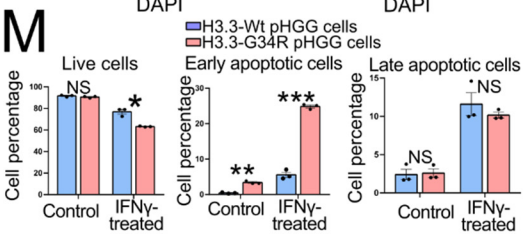

1176 **Figure 3. Epigenetic activation of the STAT pathway in G34R pHGG A)** Diagram
1177 depicting IFNγ inducing STAT1 pathway activation. GAS: interferon-gamma activated
1178 site; ISRE: interferon-stimulated response element; SXY reg: SXY regulatory module of
1179 MHC promoters; RFX: DNA-binding complex. **B)** The combination of different histone
1180 mark deposition enabled the definition and the identification of chromatin states (CS).
1181 The table shows CS changes at specific genomic regions for STAT1 pathway related
1182 genes, based on the combination of different histone mark enrichments, considering a
1183 fold-change enrichment cut-off > 2 (n=3 biological replicates). TSS=transcription start
1184 site. For each gene shown the CS number is indicated between parentheses. **C)**
1185 Heatmap illustrates RNA-Seq data of H3.3-WT (n=4) and H3.3-G34R (n=3) tumor cells
1186 from SB tumors. Heatmap shows the differential expression of some of the genes with
1187 CS changes in B). Blue=gene downregulation, Red=gene upregulation. **D-E)**
1188 Occupancy of H3K27Ac and H3K4me3 on the *Stat1* gene. The y axis of each profile
1189 represents the estimated number of immunoprecipitated fragments at each position
1190 normalized to the total number of reads in a given dataset. Reference sequence
1191 (RefSeq) gene annotations are shown in blue. **F)** Western blot of phospho-STAT1 and
1192 STAT1 at different time points after stimulation with IFN-γ, in H3.3-Wt and H3.3-G34R
1193 mouse pHGG cells. **G)** Quantification of phospho-STAT1 normalized levels from the
1194 experiment described in **F**. **H)** Western blot of phospho-JAK2 and JAK2 at basal levels
1195 and upon stimulation with IFN-γ in H3.3-Wt and H3.3-G34R mouse pHGG cells. **I)**
1196 Occupancy of H3K27Ac on the *Stat5a* and *Stat5b* genes. The y axis of each profile
1197 represents the estimated number of immunoprecipitated fragments at each position
1198 normalized to the total number of reads in a given dataset. Reference sequence

1199 (RefSeq) gene annotations are shown in blue. **J)** Western blot of phospho-STAT5a and
1200 STAT5a at basal levels and upon stimulation with IFN-γ in H3.3-Wt and H3.3-G34R
1201 mouse pHGG cells. **K)** Heatmap of a protein array showing the relative normalized PTM
1202 levels of JAK/STAT related proteins in G34R mouse pHGG cells versus H3.3-WT cells,
1203 highlighting the main upregulated and downregulated proteins and PTMs. **L)** H3.3-
1204 G34R or H3.3–WT neurospheres were incubated with IFNγ (200 UI) or diluent (control)
1205 and apoptosis was measured at 48 hours by AnnexinV and DAPI staining. **M)**
1206 Percentages of live cells, early apoptotic cells and late apoptotic cells after IFNγ-
1207 treatment in H3.3-Wt and H3.3-G34R mouse pHGG cells. *P < 0.05, **P < 0.01, ***P <
1208 0.005, and ****P < 0.001, unpaired t test.

1209

1210

1211

1212

1213

1214

1215

1216

1217

1218

Figure 4 - Upregulation of MHC-I expression in H3.3-G34R pHGG

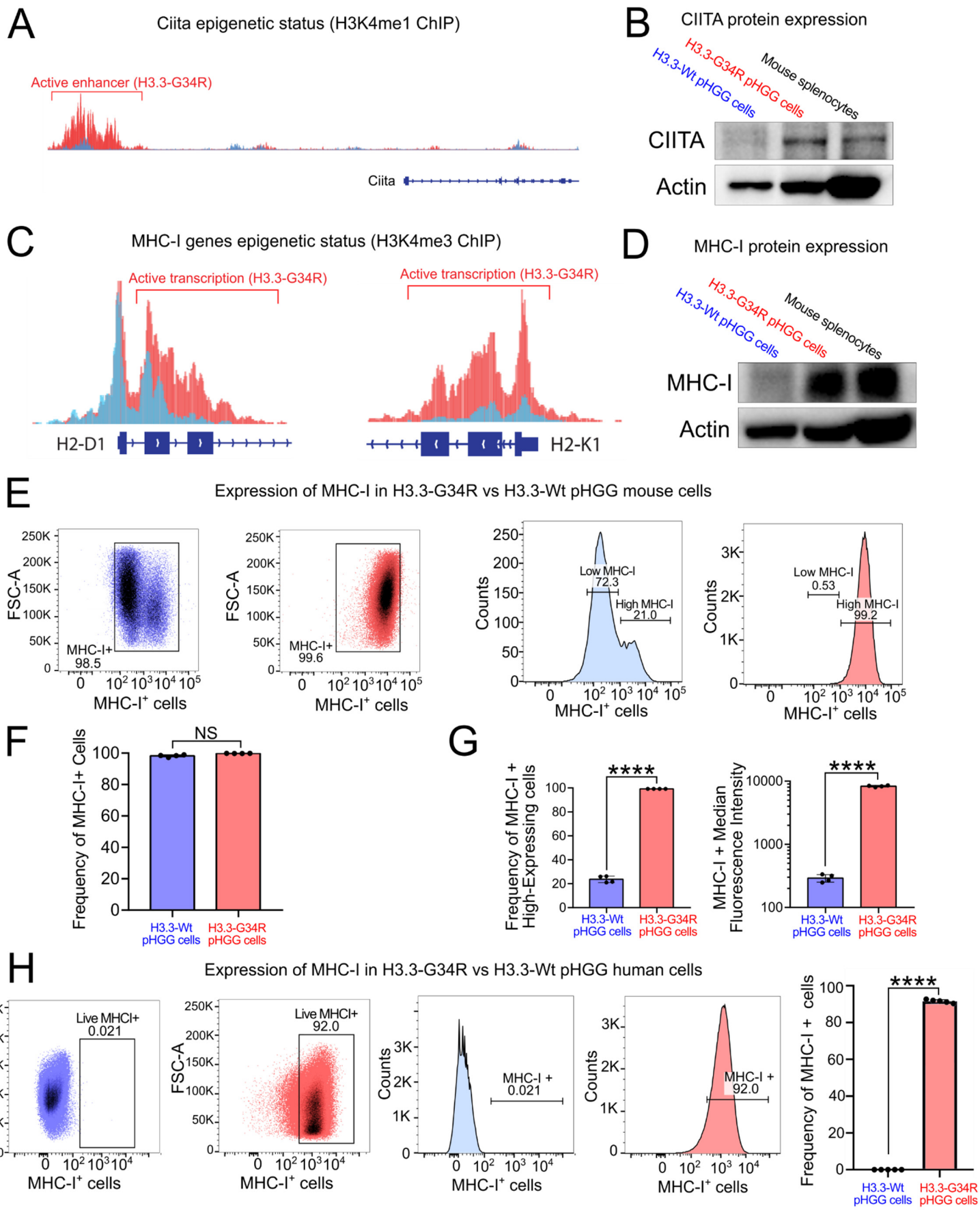

1237 **Figure 4. Expression of MHC-I in H3.3-G34R vs H3.3-Wt pHGG A)** Occupancy of
1238 H3K4me1 on the *Ciita* gene. The y axis of each profile represents the estimated number
1239 of immunoprecipitated fragments at each position normalized to the total number of
1240 reads in a given dataset. Reference sequence (RefSeq) gene annotations are shown in
1241 blue. **B)** Western blot for CIITA at basal levels and upon treatment with IFN-γ in H3.3-
1242 Wt and H3.3-G34R mouse pHGG cells. Mouse splenocytes were included as positive
1243 CIITA expressing cells control. C**)** Occupancy of H3K4me3 on the MHC-I genes H2-D1
1244 and H2-K1. The y axis of each profile represents the estimated number of
1245 immunoprecipitated fragments at each position normalized to the total number of reads
1246 in a given dataset. Reference sequence (RefSeq) gene annotations are shown in blue.
1247 **D)** Western blot for MHC-I at basal levels and upon treatment with IFN-γ in H3.3-Wt and
1248 H3.3-G34R mouse pHGG cells. Mouse splenocytes were included as positive CIITA
1249 expressing cells control. **E)** Expression of MHC-I in mouse pHGG cells by flow
1250 cytometry. **F-G)** Quantitative analysis of the experiment shown in E). **H)** Expression of
1251 MHC-I in mouse pHGG cells by flow cytometry and Quantitative analysis of the
1252 experiment. ****$P < 0.001$, unpaired t test.

1253

1254

1255

1256

1257

1258

Figure 5 - Transcriptional analysis of H3.3-G34R pHGG TME immune cells

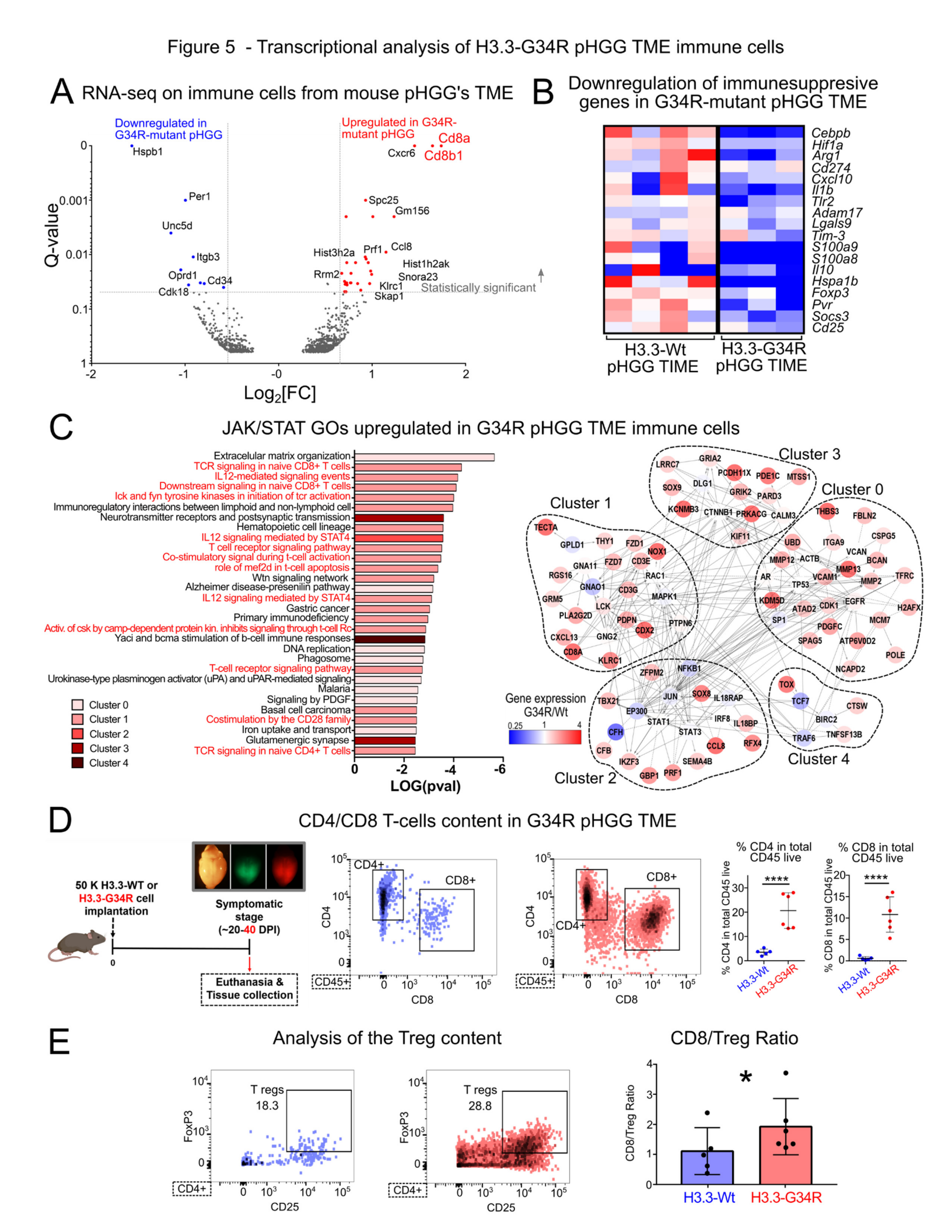

1277 **Figure 5. Transcriptional analysis of H3.3-G34R pHGG TME immune cells. A)**
1278 Volcano plot shows differentially expressed genes (-Log(p-value), y axis) versus the
1279 magnitude of change or fold change (Log2(Fold Change), x axis) when comparing gene
1280 expression in 0.CD45 cells derived from H3.3-G34R versus CD45 from H3.3-WT SB-
1281 generated tumors. CD45 cells were magnetically sorted from H3.3-G34R and H3.3-WT
1282 SB-tumors and their RNA was purified for RNA-Seq analysis. **B)** Heatmap shows the
1283 expression level of genes related to immunosuppression in CD45+ cells obtained from
1284 H3.3-G34R and H3.3-WT SB-derived tumors. **C)** Plot showing the 30 most significant
1285 enriched pathways (x-axis) in terms of p-value (-Log(p-value), y-axis). Pathways related
1286 to T-cell activation and function are highlighted in red; and network analysis of
1287 differentially upregulated genes in H3.3-G34R CD45 cells with respect to H3.3-WT
1288 CD45 cells. Clusters of nodes of identical color represent a cluster of genes involved in
1289 similar biological pathways. Linker genes have been used to construct the network and
1290 they are depicted in red. Numbers indicate the cluster number. **D)** Illustration of
1291 experimental procedure followed for the characterization of T cells in H3.3-G34R mouse
1292 pHGG TME. Fifty thousand H3.3-WT or H3.3-G34R neurospheres were implanted in
1293 C57BL6 mice and, at symptomatic stage, the immune cell infiltration was characterized.
1294 Total pan T cells were identified as CD45+/CD3+ cells and further classified by the
1295 expression of CD8 or CD4 (CD45+/CD3+/CD8+ or CD45+/CD3+/CD4+, respectively).
1296 **E)** CD4+ T cells were sub-classified as regulatory T cells (Tregs)
1297 (CD45+/CD3+/CD4+/FoxP3+CD25+). The ratio of the percentage of CD8+ T cells to
1298 Tregs in total CD45+ subset was calculated in each sample and plotted. H3.3-G34R

1299 TME had an increased effector CD8+ T cells:Treg ratio than the H3.3-WT TME. ***
1300 $p<0.001$; * $p<0.05$; Student T test.

1301

1302

1303

1304

1305

1306

1307

1308

1309

1310

1311

1312

1313

1314

1315

1316

1317

Figure 6 - Analysis of the TIME of H3.3-G34R pHGG

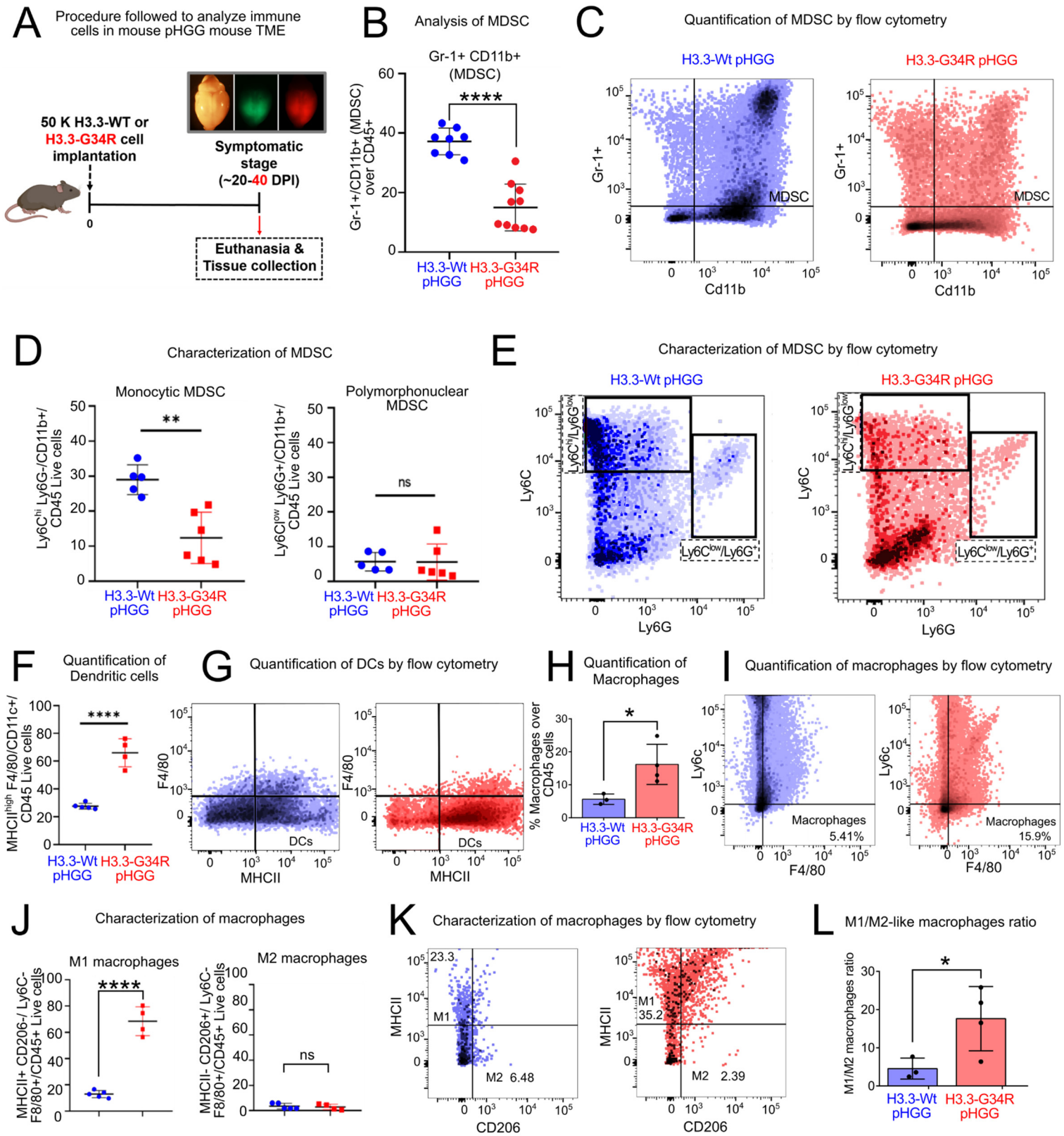

1336 **Figure 6. Analysis of the tumor microenvironment (TIME) of H3.3-G34R pHGG. A)**
1337 Experimental outline: fifty thousand H3.3-WT or H3.3-G34R neurospheres were
1338 implanted in C57BL6 mice and, at symptomatic stage, the immune cell infiltration was
1339 characterized. **B-C)** The proportion of cells with myeloid derived suppressor cell
1340 phenotype (CD45+/Gr-1+ CD11b+) as well as their **D-E**) sub-characterization into
1341 Polymorphonuclear (CD45+/CD11b+/Ly6G+Ly6Clo) or Monocytic
1342 (CD45+/CD11b+/Ly6G-Ly6Chi) was performed on H3.3-WT and H3.3-G34R TMEs. **F-**
1343 **G)** The total proportion of dendritic cells is shown as the percentage of
1344 CD45+/CD11c+/F4/80+MHCIIhi cells. **H-I)** Macrophage were identified as CD45+/Ly6C-
1345 F4/80+ cells and were further classified as **J-L)** M1 (CD45+/Ly6C-
1346 F4/80+/MHCII+CD206-) or M2 (CD45+/Ly6C-F4/80+/MHCII-CD206+) (left panel). The
1347 M1/M2 ratio was calculated for H3.3-WT and H3.3-G34R TMEs (right panel). ****
1348 p<0.0001; ***p<0.001, **p<0.01 * p<0.05; ns = non-significant; Student T test.

1349

1350

1351

1352

1353

1354

1355

1356

Figure 7 - Cytokines profile of G34R pHGG cells and immune properties of the conditioned media

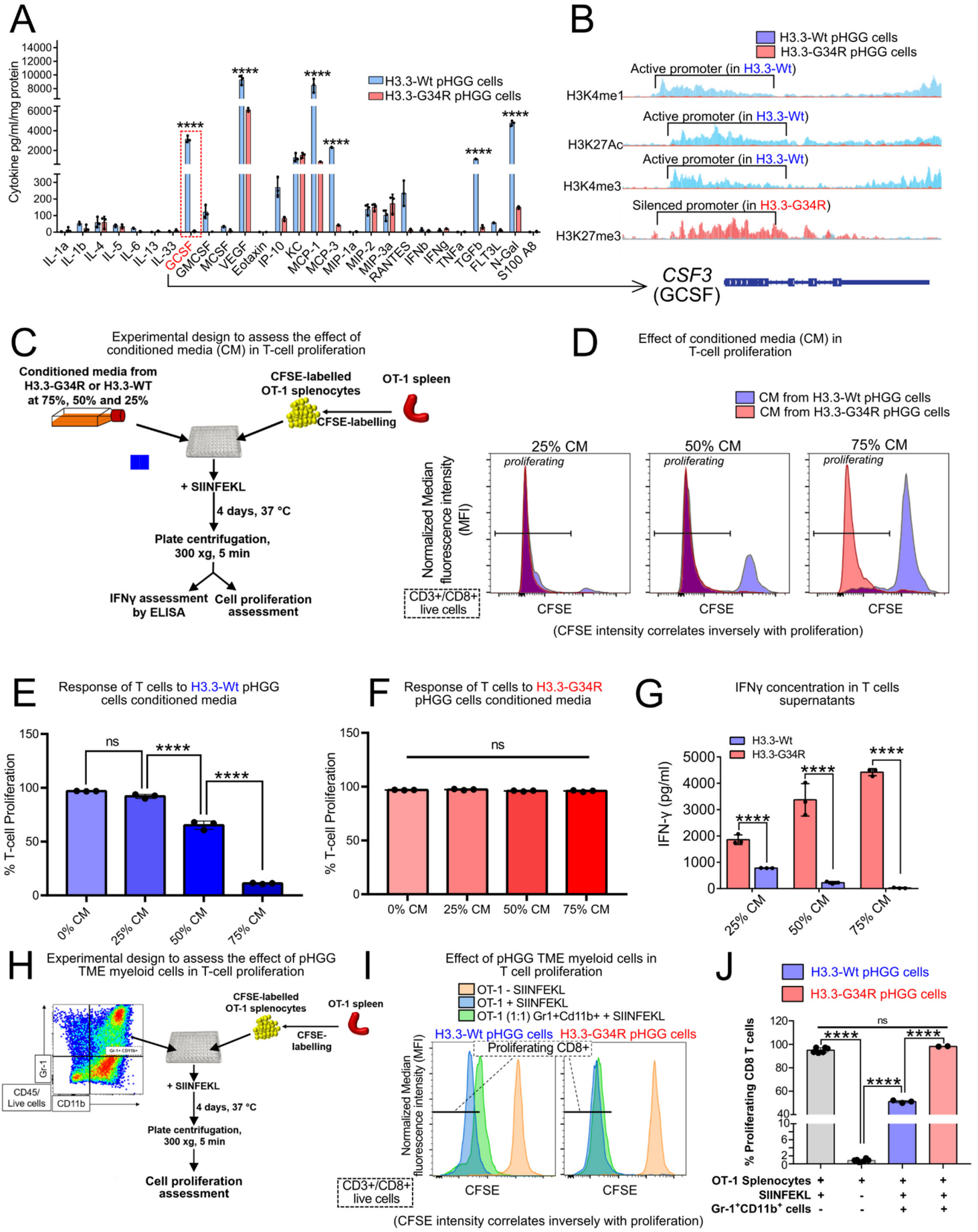

1375 **Figure 7. Cytokines profile of G34R pHGG cells and immune properties of the**
1376 **conditioned media. A)** To assess the concentration of different cytokines, three
1377 different clones of H3.3-WT and H3.3-G34R neurospheres (1x106 cells/flask) were
1378 seeded in T25 flasks and 48 hours later, conditioned media was analyzed by ELISA.
1379 Total protein present in each flask was determined and cytokine concentration was
1380 normalized to protein quantity. ****$p<0.0001$, 2-way ANOVA and Sidak's multiple
1381 comparisons test. **B)** The plots show the occupancy of H3K27me3 (transcriptional
1382 repressing), H3K27ac, H3K4me3 and H3K4me1 (transcriptional activating) histone
1383 marks on the G-CSF (*Csf3*) promoter region (light blue dashed box). The y axis of each
1384 profile represents the estimated number of immunoprecipitated fragments at each
1385 position normalized to the total number of reads in a given dataset. Reference
1386 sequence (RefSeq) gene annotation is shown in blue. The overlay of called peaks in
1387 n=3 biological replicates of H3.3-G34R neurospheres is shown in red whereas the
1388 overlay of the called peaks from n=3 H3.3-WT neurospheres is shown in light blue. **C)**
1389 Experimental layout of the T cell proliferation assay to test the immunosuppressive
1390 capacity of conditioned media (CM) from H3.3-G34R or H3.3-WT neurospheres. Fifty
1391 thousand OT-1 splenocytes previously labeled with CFSE were incubated with 0%,
1392 25%, 50% or 75% of CM and SIINFEKL, the specific peptide to stimulate OT-1 CD8 T
1393 cell proliferation, was added at a concentration of 100 nM. Cells were incubated for 4
1394 days at 37 °C. T cell proliferation was measured as the reduction of CFSE staining in
1395 the CD45+/CD3+/CD8+ population with respect to the positive control of OT-1
1396 splenocytes + SIINFEKL. **D)** Representative histograms show the CD8+ T cell
1397 proliferation in the presence of 25%, 50% or 75% CM from H3.3-G34R or –WT

1398 neurospheres. The green triangle and the blue triangle below the histograms represent
1399 the intensity of CFSE staining and the proliferation rate interpretation, respectively. **E-F)**
1400 Bars represent the percentage of proliferating CD8+ T cells in the presence of CM from
1401 **E)** H3.3-WT or **F)** H3.3-G34R neurospheres, with respect to the positive control (0%
1402 CM). **G)** IFNγ concentration was measured in the supernatant of the cultures by ELISA.
1403 Bars represent cytokine concentration in absolute numbers. **H)** Experimental layout of
1404 the T cell proliferation assay to test the immunosuppressive capacity of Gr-1+ CD11b+
1405 cells isolated from H3.3-WT and H3.3-G34R tumor microenvironments (TMEs). Fifty
1406 thousand H3.3-WT or –G34R neurospheres were implanted in C57BL6 mice and at
1407 symptomatic stage, animals were euthanized and Gr-1+ CD11b+ cells (MDSC
1408 phenotype) were FACS-sorted from the TMEs and co-cultured 1:1 with OT-1
1409 splenocytes previously labeled with CFSE. SIINFEKL, was added at a concentration of
1410 100 nM and cells were incubated for 4 days at 37 °C. **I)** T cell proliferation was
1411 measured as the reduction of CFSE staining in the CD45+/CD3+/CD8+ population with
1412 respect to the positive control (OT-1 splenocytes + SIINFEKL). Upper panel:
1413 Representative histograms showing the CD8+ T cell proliferation in the presence of Gr-
1414 1+ CD11b+ cells from H3.3-WT and H3.3-G34R TMEs. The green triangle and the blue
1415 triangle below the histograms represent the intensity of CFSE staining and the
1416 proliferation rate interpretation, respectively. **J)** Bars represent the percentage of
1417 proliferating CD8+ T cells in each treatment with respect to the positive control (OT-1
1418 splenocytes + SIINFEKL)**. I)** IFNγ concentration was measured in the supernatant of the
1419 co-cultures by ELISA. Bars represent IFNγ concentration in absolute numbers. The
1420 insert shows IFNγ secretion in the control wells (OT-1 +/- SIINFEKL). *** $p<0.001$, ***

1421 p<0.001; ns=non-significant; ANOVA and Tukey test. **** p<0.0001; ns=non-significant;
1422 ANOVA and Tukey test; mean ± SEM.
1423
1424
1425
1426
1427
1428
1429
1430
1431
1432
1433
1434
1435
1436
1437
1438
1439

Figure 8 - Evaluation immunological memory in gene therapy long term survivors rechallenged with G34R-mutant pHGG cells

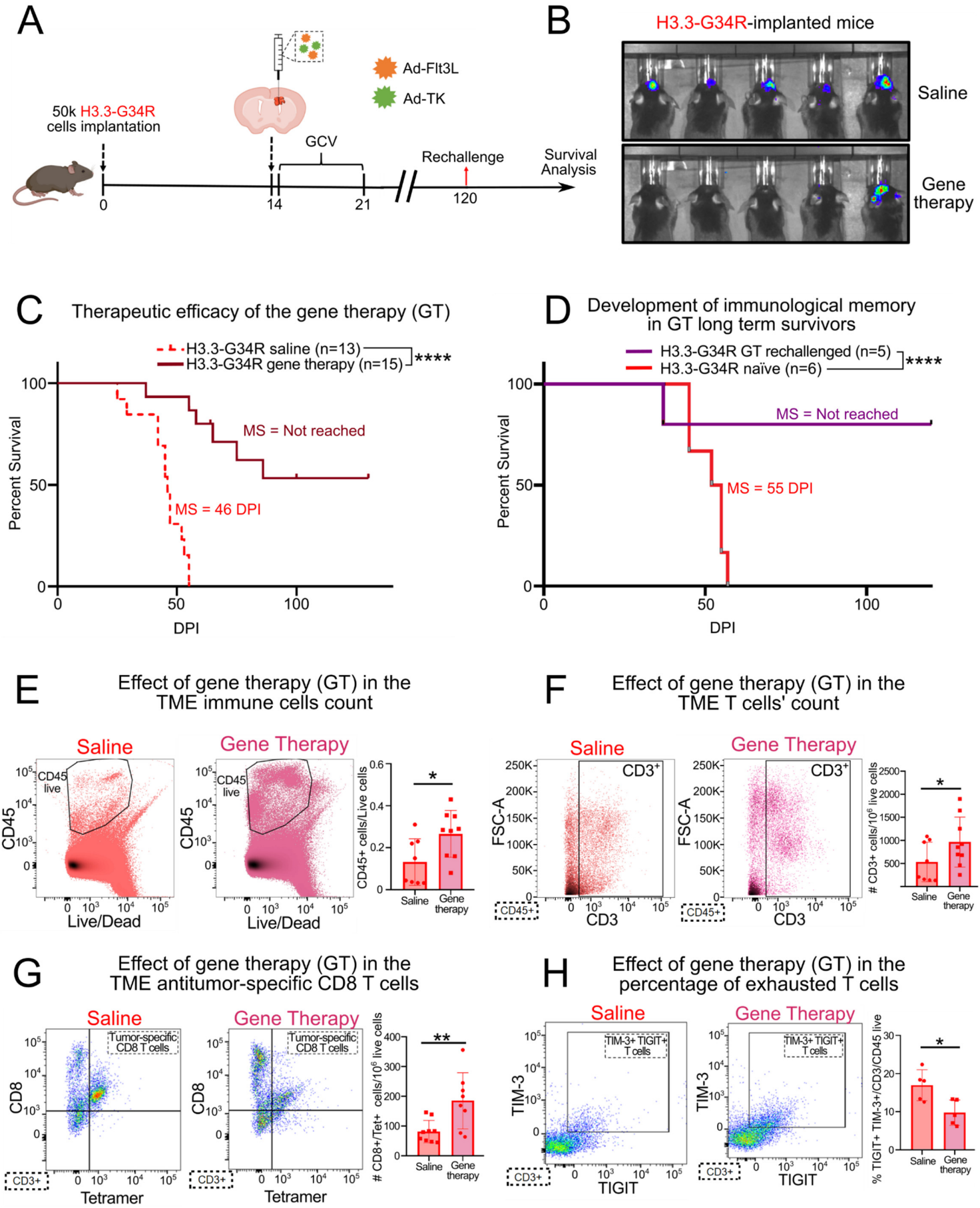

1458 **Figure 8. Evaluation of a GCV-inducible gene therapy for H3.3-G34R pHGG A)**
1459 Diagram depicting the experimental outline for the treatment of H3.3-G34R tumor
1460 bearing mice with Ad-Flt3L + Ad-TK gene therapy (GT). Treatment of H3.3-G34R tumor
1461 bearing mice was done at 14 DPI. The day after the administration of the Ad-Flt3L + Ad-
1462 TK therapy, ganciclovir (GCV) (25 µg/gr mouse) was delivered, twice a day, for 7
1463 consecutive days. Animals were euthanized at symptomatic stage. **B)** IVIS scan of
1464 animals bearing H3.3-G34R tumors 14 days after being treated with Saline or GT. **C)**
1465 Kaplan-Meier survival curve for the GT experiment. Median survival (MS) and number
1466 of animals used are detailed in the plot legend. *** $p<0.001$, Mantel-Cox test **D)** Long-
1467 term survivors were implanted in the contralateral hemisphere with 50.000 H3.3-G34R
1468 cells and animals were euthanized at symptomatic stage. **E)** Percentage of CD45
1469 infiltration in the TME of H3.3-G34R tumor bearing mice treated with Saline or GT. F)
1470 Number of T cells (CD45+ CD3+) in the TME of H3.3-G34R tumor bearing mice treated
1471 with Saline or GT, per 1 million total live cells. **G)** Number of tumor-specific CD8 T cells
1472 (CD45+ CD3+ CD8+ Tet+) in the TME of H3.3-G34R tumor bearing mice treated with
1473 Saline or GT, per 1 million total live cells. **H)** Percentage of double positive T cells for
1474 TGIT and TIM-3, two T cell exhaustion markers. * $p<0.05$; ** $p<0.01$ Student T test.

1475

1476

1477

1478

1479